Supporting Information for:

Chemical and Electrochemical Properties of [Cp*Rh] Complexes Supported by a Hybrid Phosphine-Pyridine Ligand

*Julie A. Hopkins, Davide Lionetti, Victor W. Day, and James D. Blakemore**

Department of Chemistry, University of Kansas, 1251 Wescoe Hall Drive, Lawrence, Kansas 66045, United States

*E-mail: blakemore@ku.edu (J.D.B.)

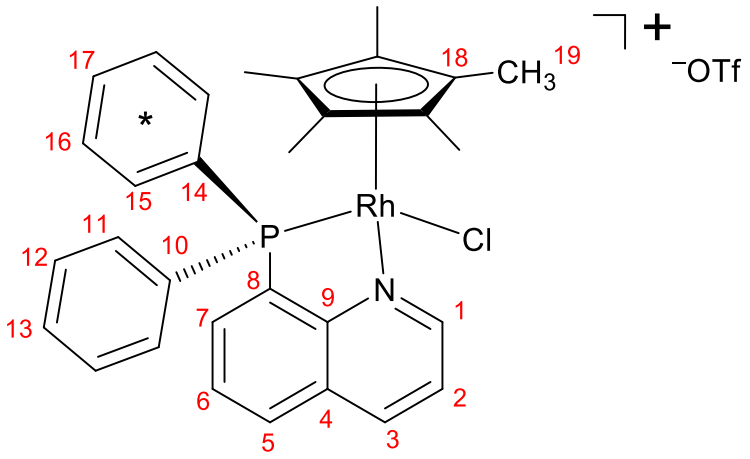

Figure S1. Numbering scheme for assignment of NMR data for complex **1-Cl** (* in ring denotes phenyl group closest to Cp* ring).

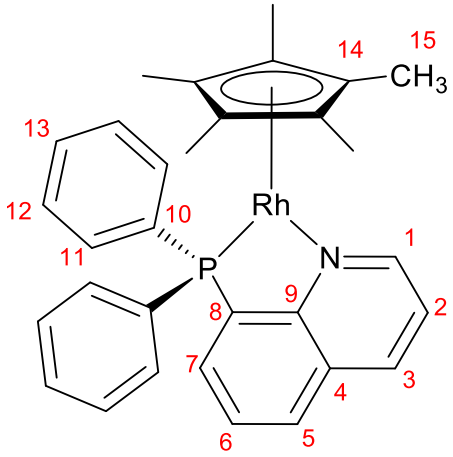

Figure S2. Numbering scheme for assignment of NMR data for complex **2**.

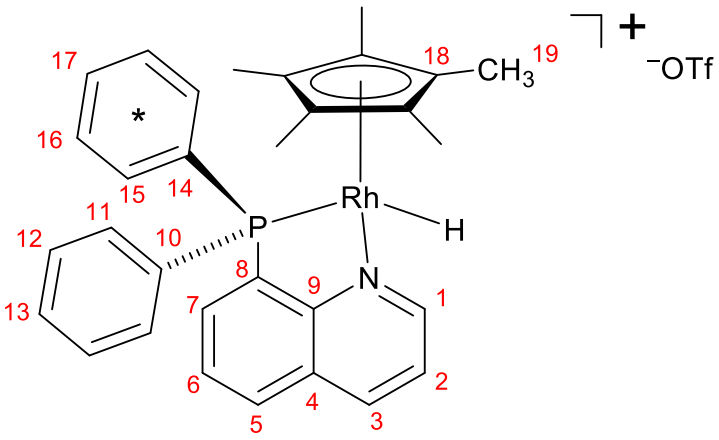

Figure S3. Numbering scheme for assignment of NMR data for complex **3** (* in ring denotes phenyl group closest to Cp* ring).

NMR Spectra

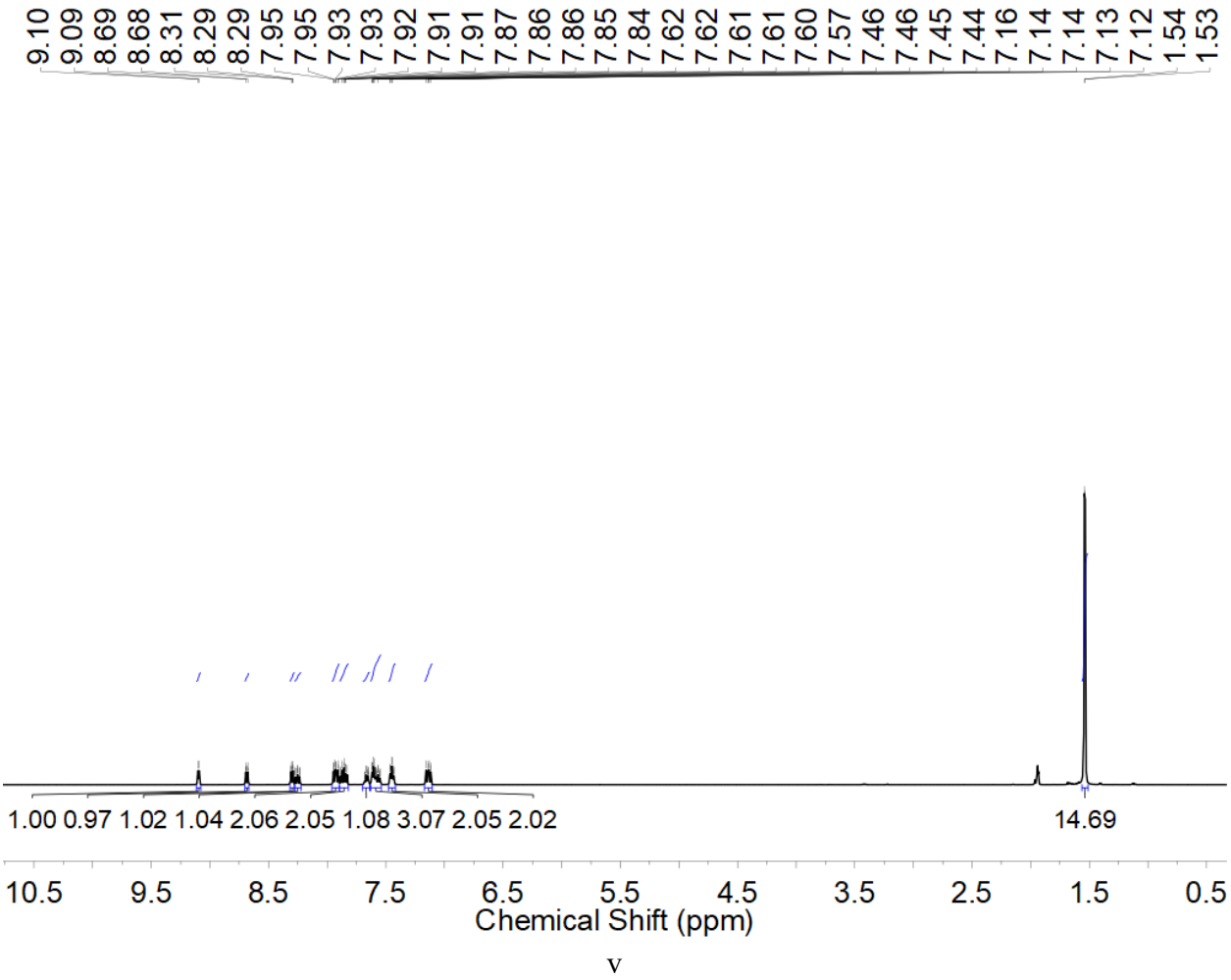

v

Figure S4. ^{1}H NMR spectrum (500 MHz, CD_3CN) of **1-Cl**.

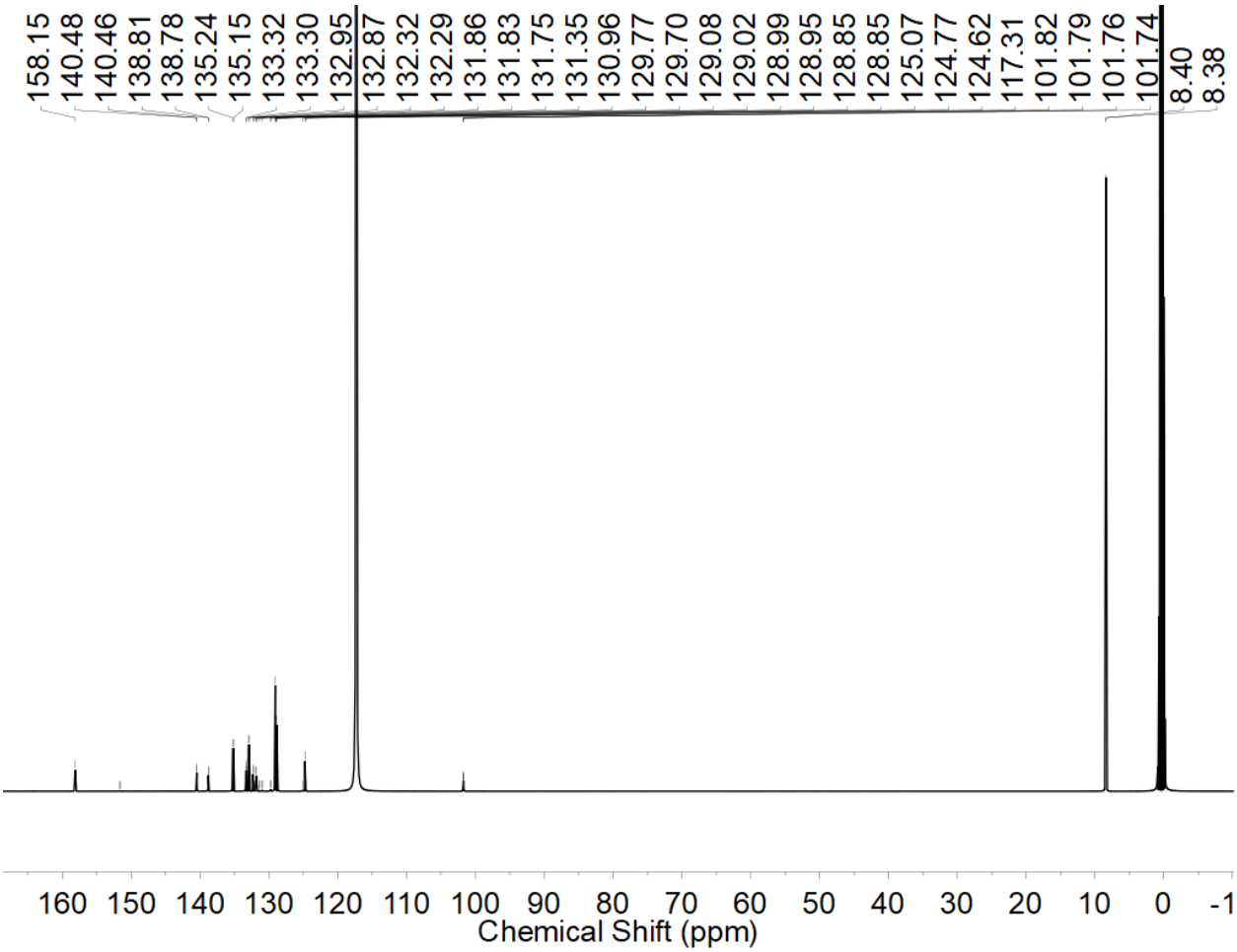

Figure S5. $^{13}C\{^{1}H\}$ NMR spectrum (126 MHz, CD_3CN) of **1-Cl**.

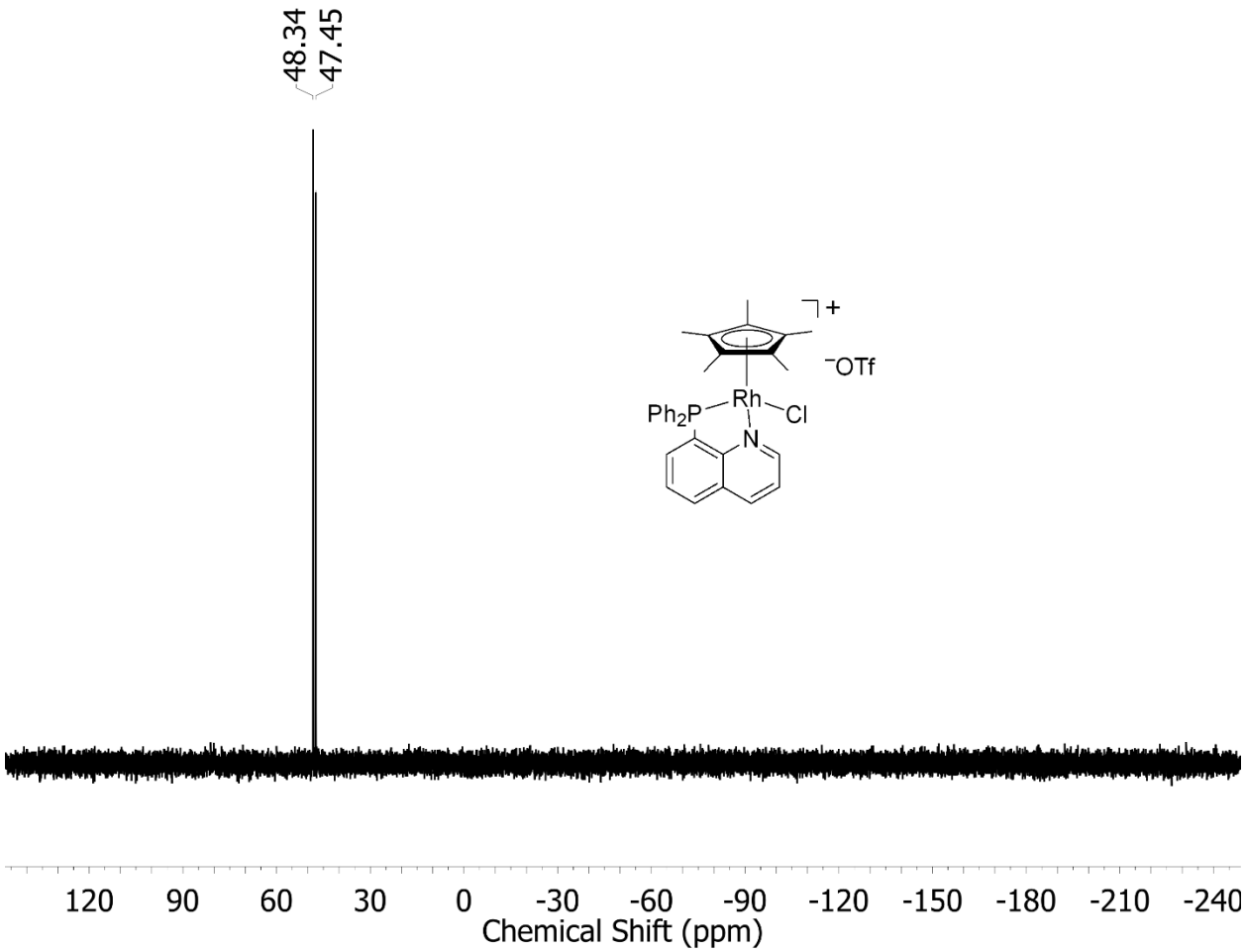

Figure S6. $^{31}P\{^{1}H\}$ NMR spectrum (162 MHz, CD_3CN) of **1-Cl**.

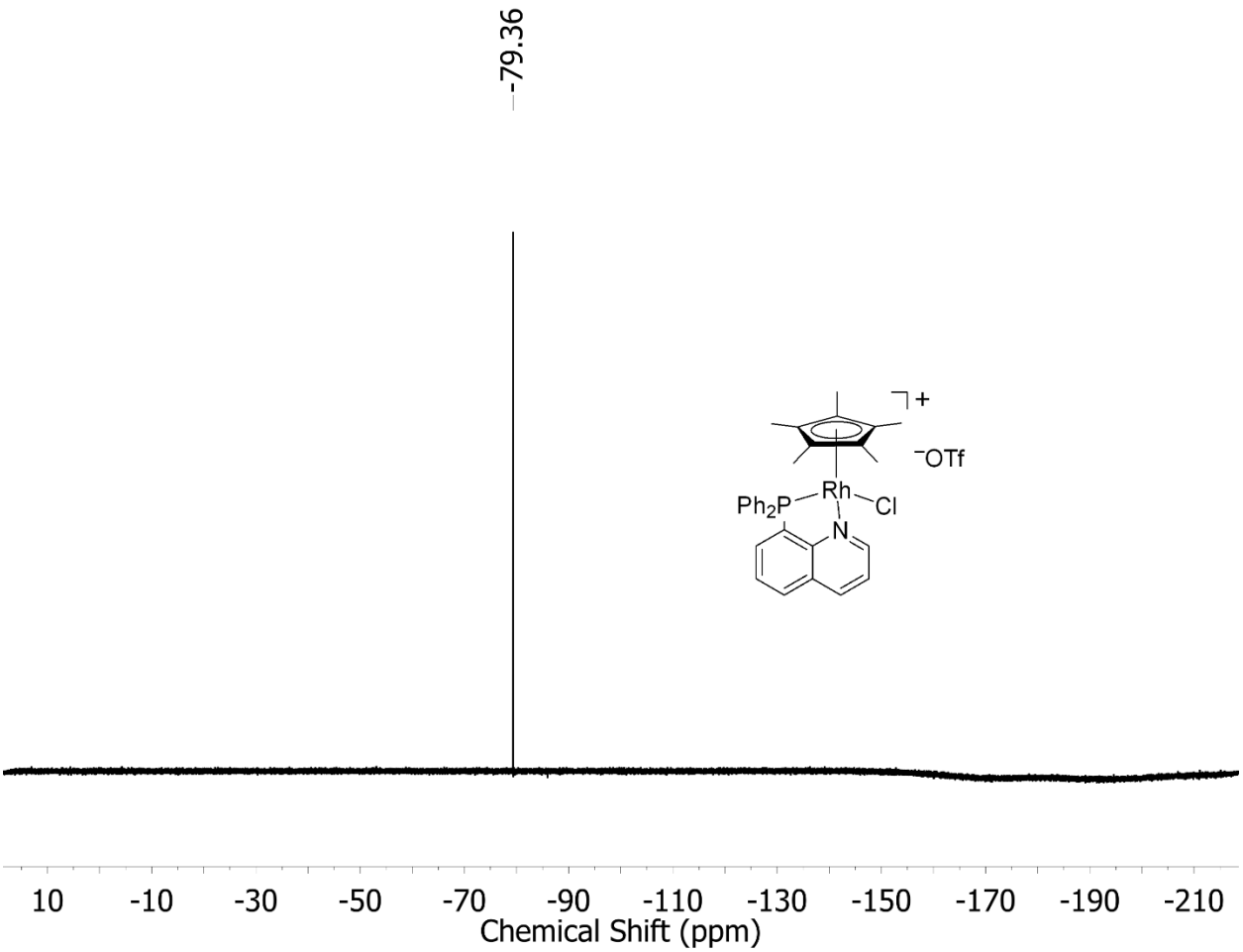

Figure S7. ^{19}F NMR spectrum (376 MHz, CD_3CN) of **1-Cl**.

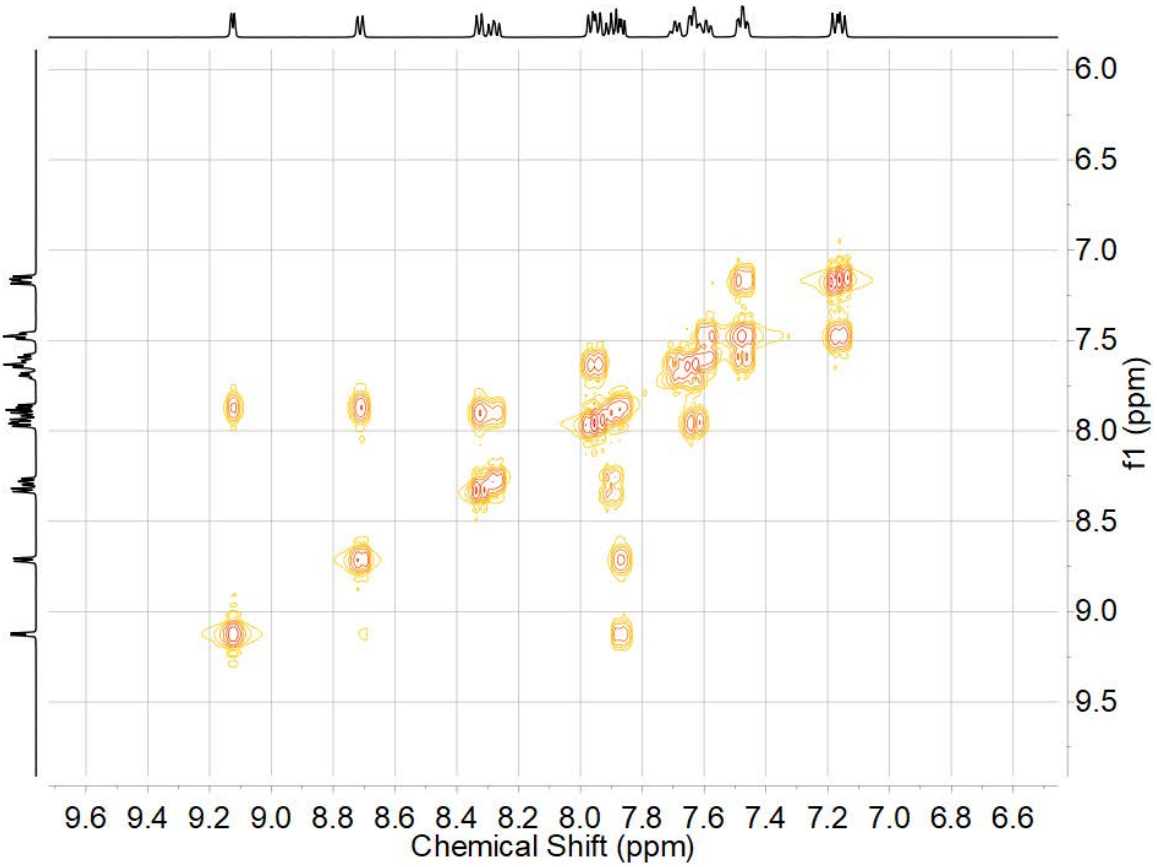

Figure S8. COSY NMR spectrum (CD_3CN) of **1-Cl**.

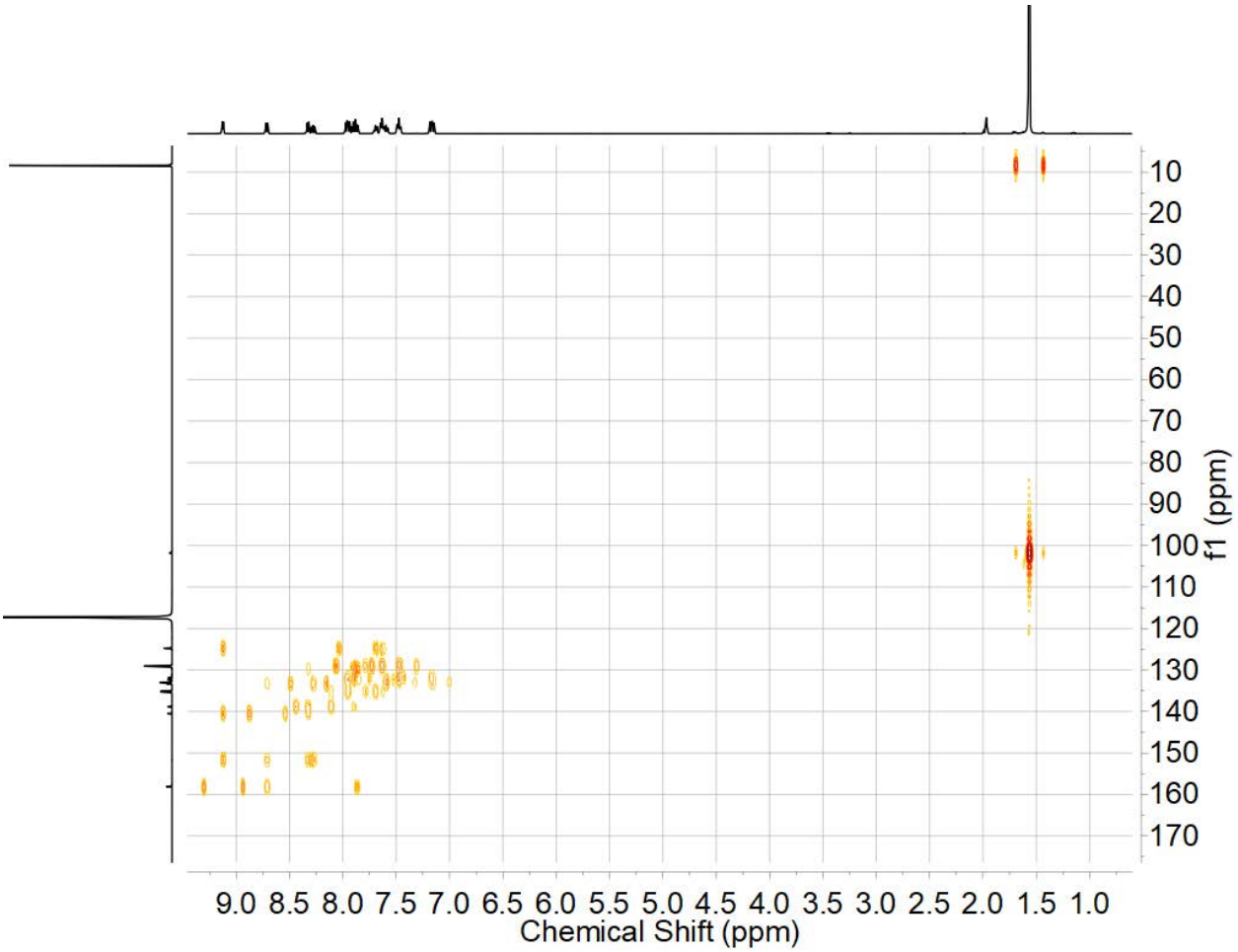

Figure S9. HMBC NMR spectrum (CD_3CN) of **1-Cl**.

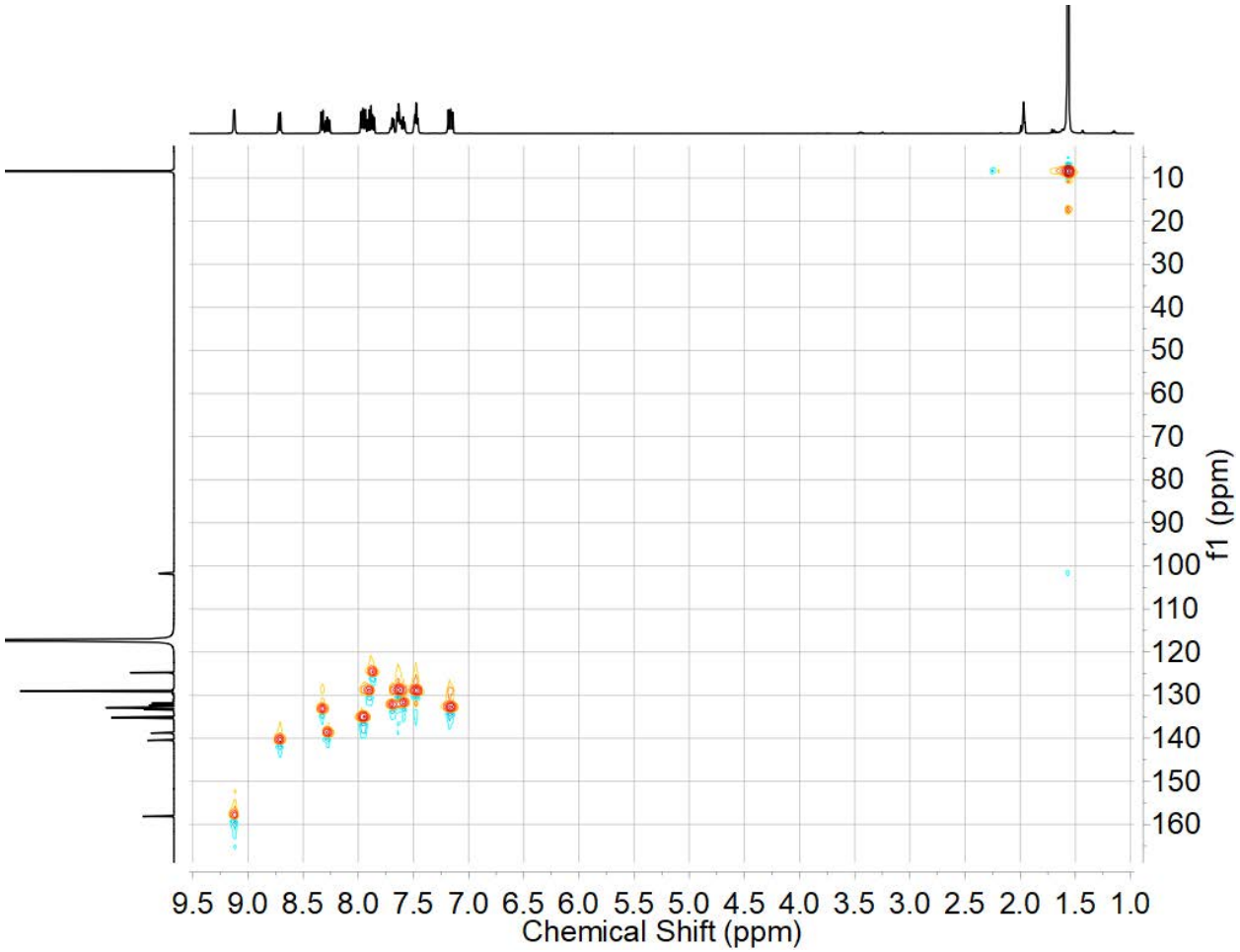

Figure S10. HSQC NMR spectrum (CD_3CN) of **1-Cl**.

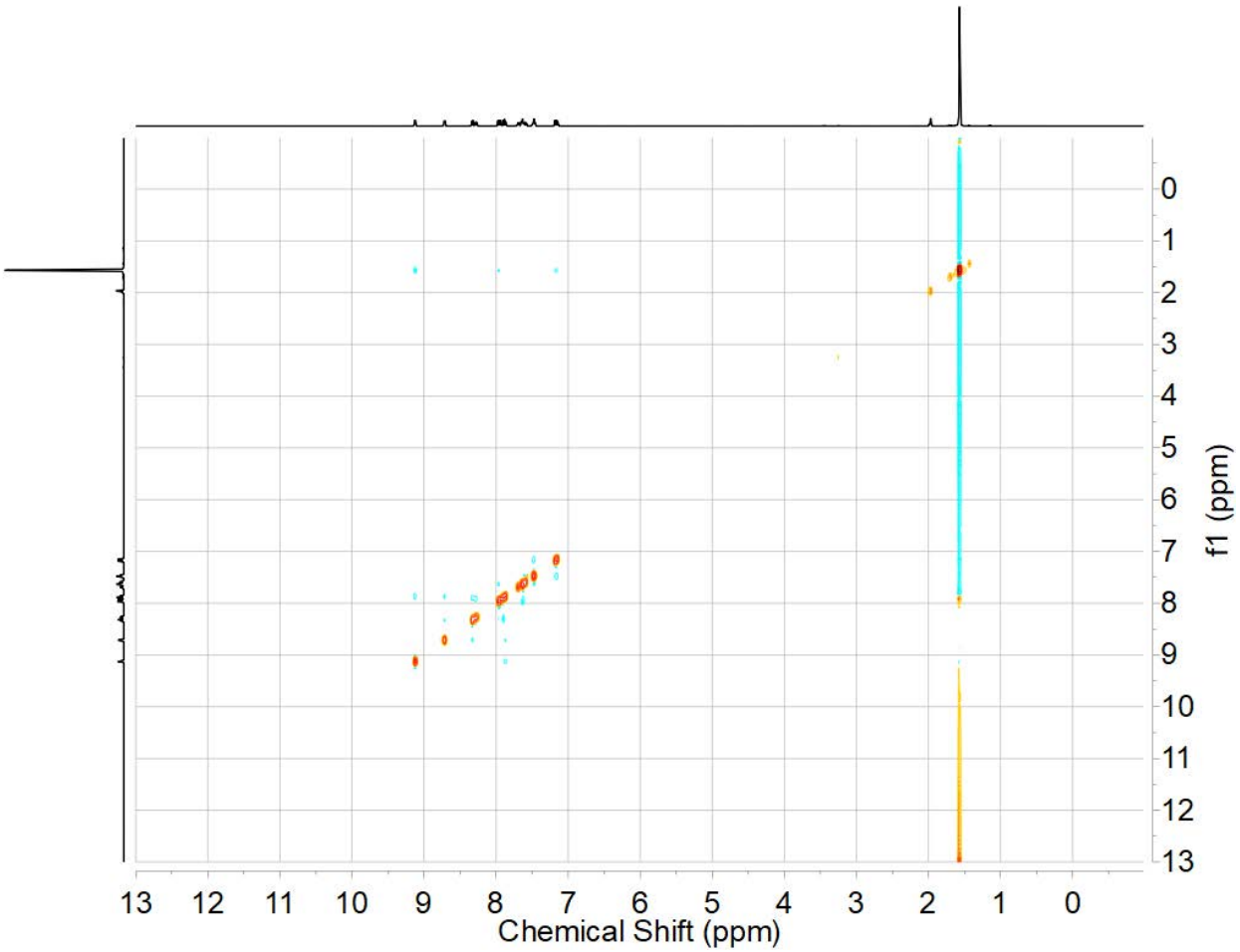

Figure S11. NOESY NMR spectrum (CD_3CN) of **1-Cl**.

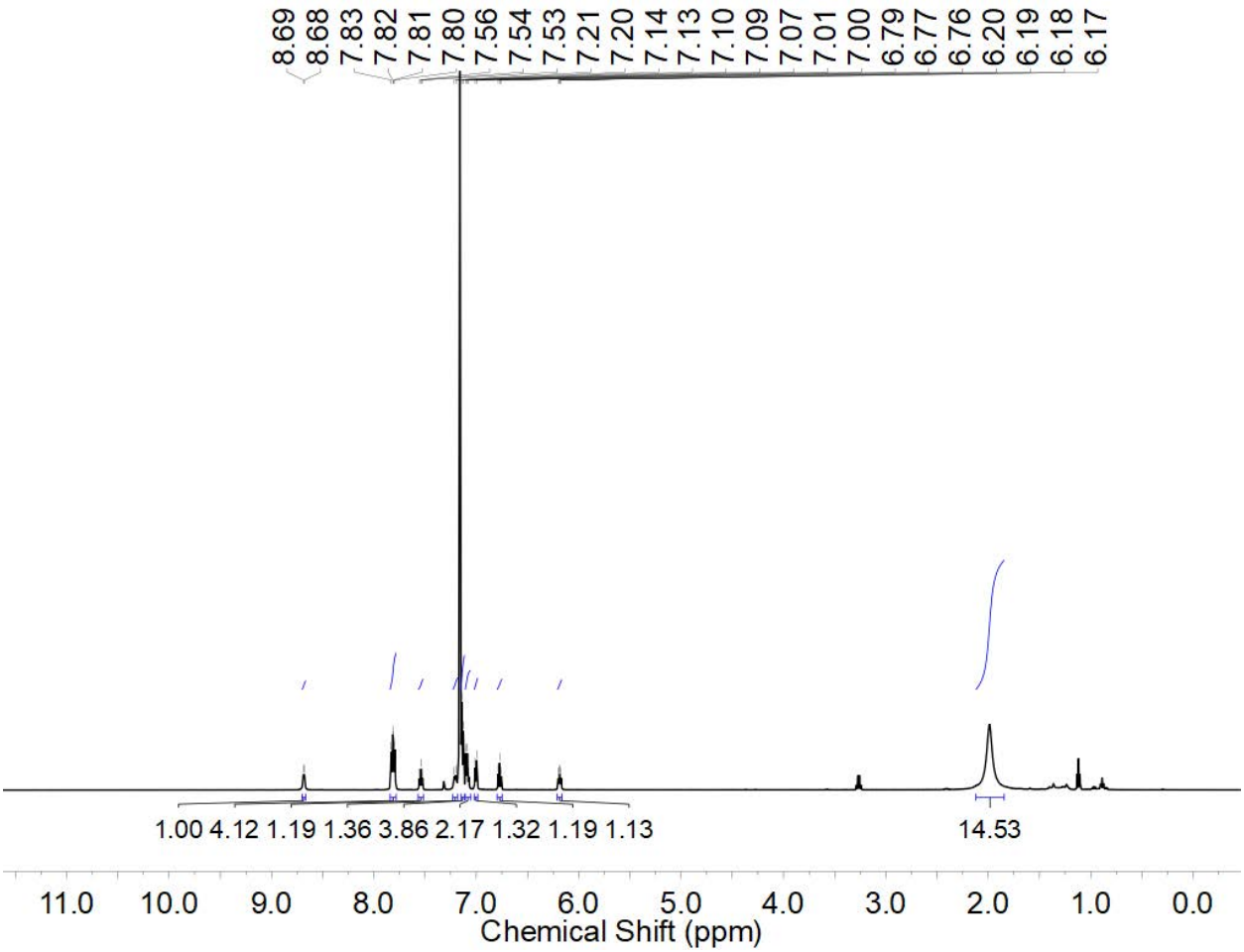

Figure S12. ^{1}H NMR spectrum (500 MHz, C_6D_6) of **2**.

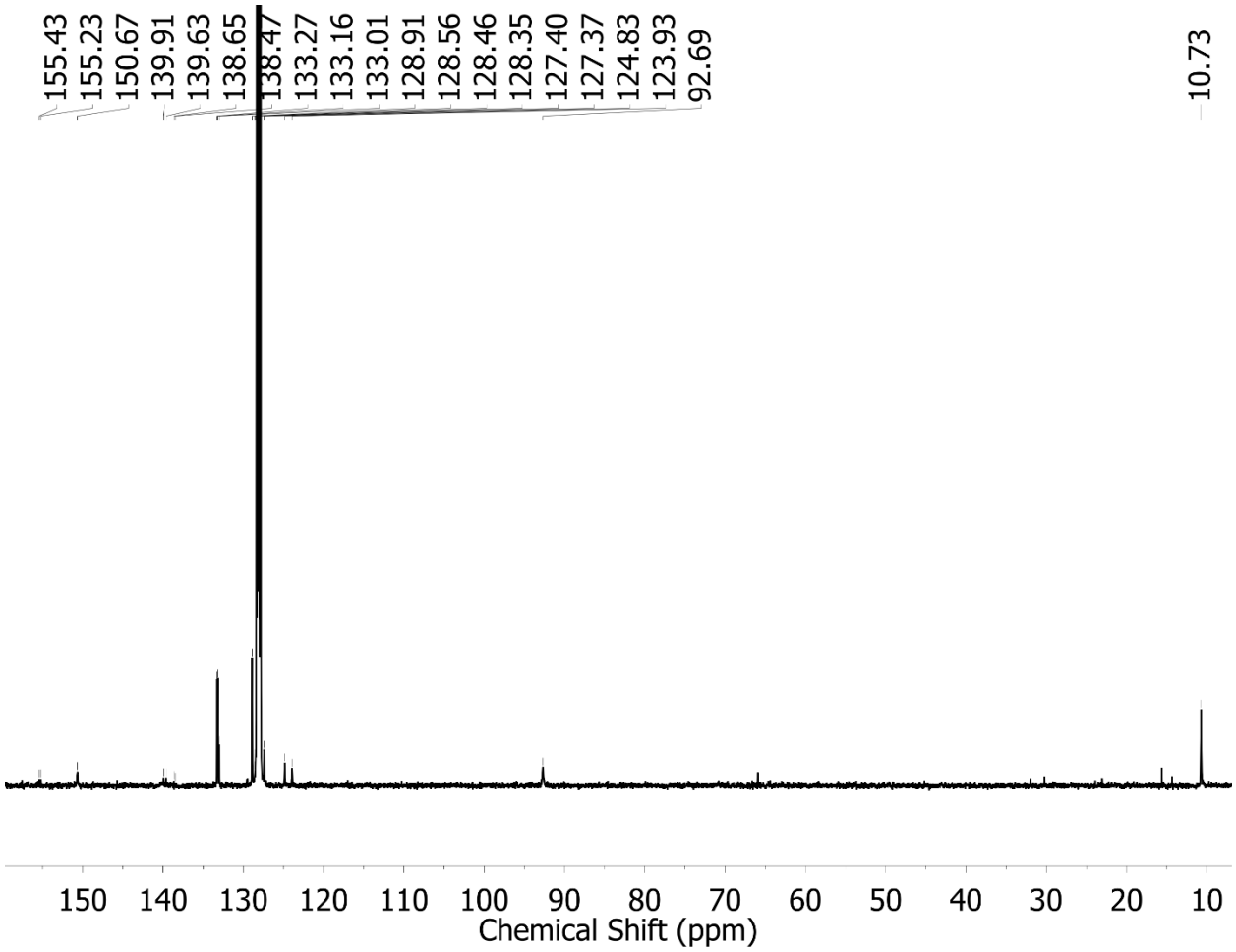

Figure S13. $^{13}C\{^{1}H\}$ NMR spectrum (126 MHz, C_6D_6) of **2**.

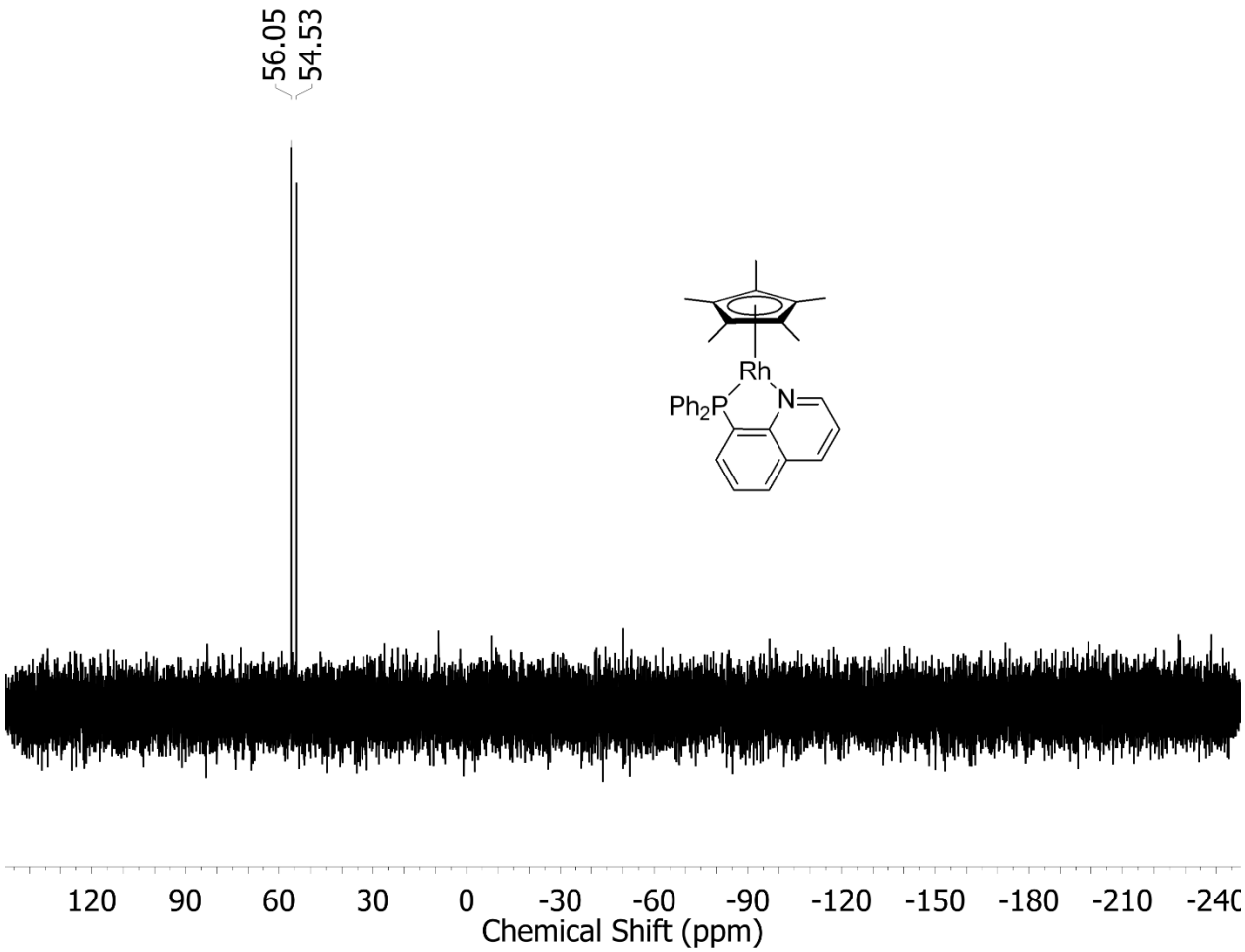

Figure S14. $^{31}P\{^{1}H\}$ NMR spectrum (162 MHz, C_6D_6) of **2**.

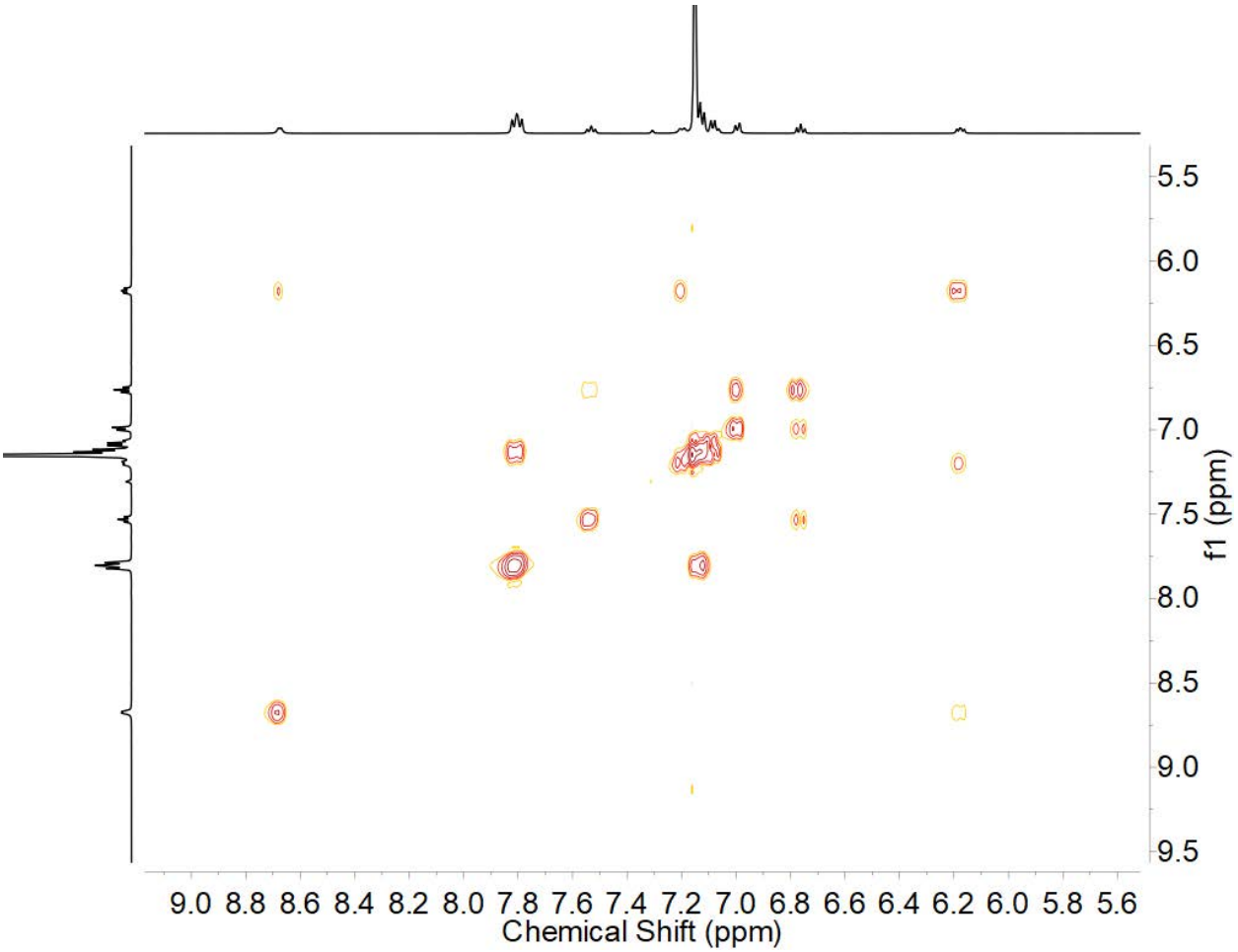

Figure S15. COSY NMR spectrum (C_6D_6) of **2**.

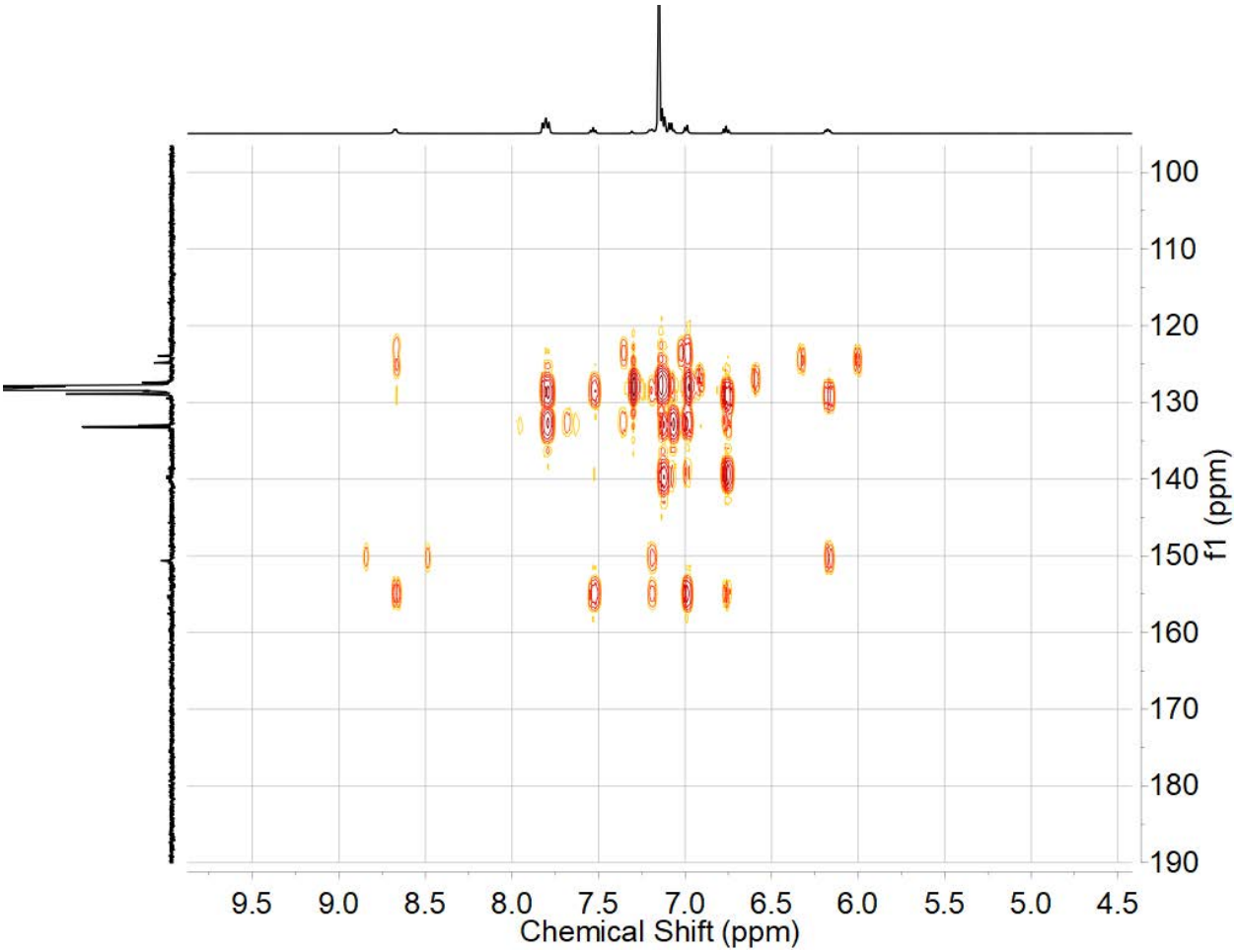

Figure S16. HMBC NMR spectrum (C_6D_6) of **2**.

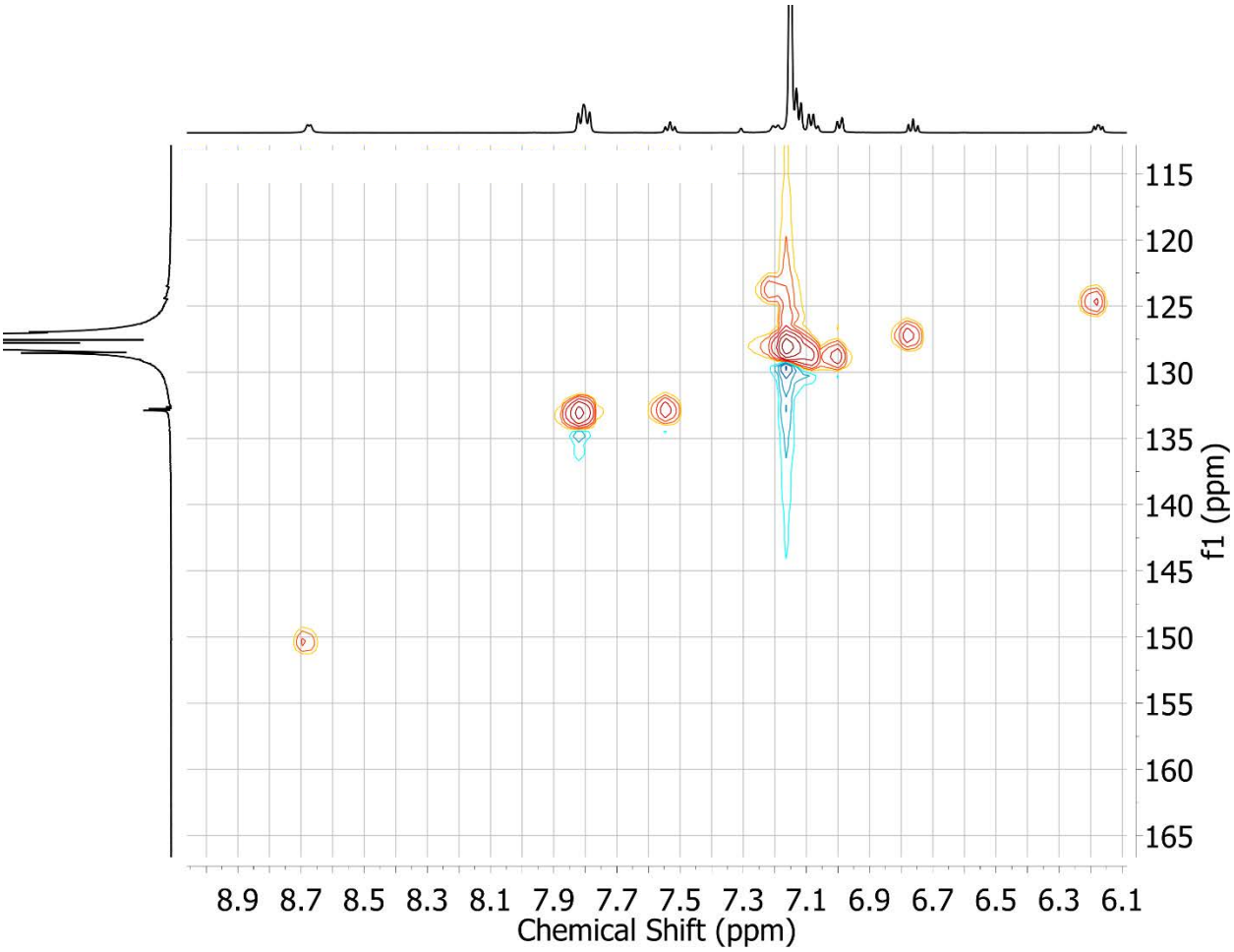

Figure S17. HSQC NMR spectrum (C_6D_6) of **2**.

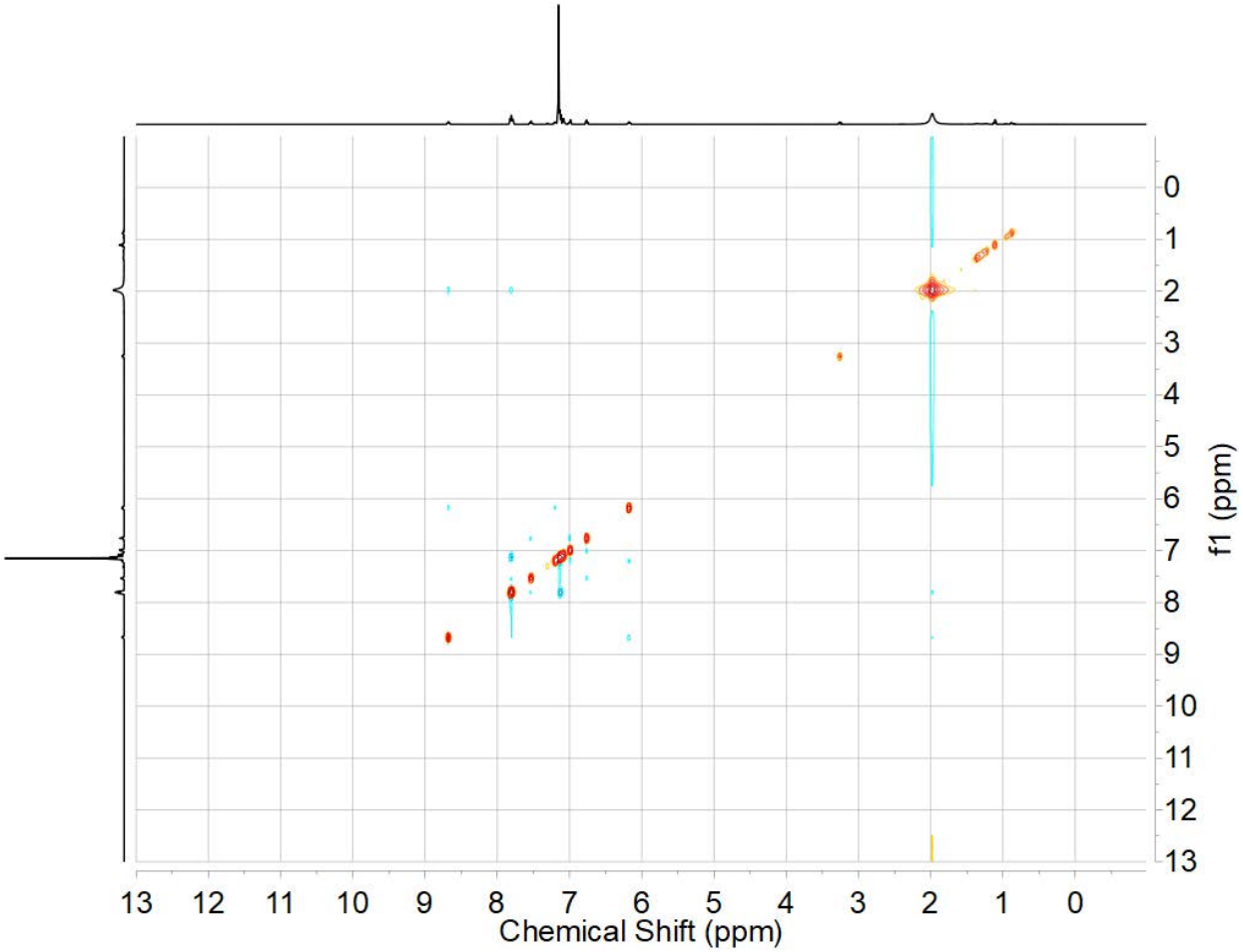

Figure S18. NOESY NMR spectrum (C_6D_6) of **2**.

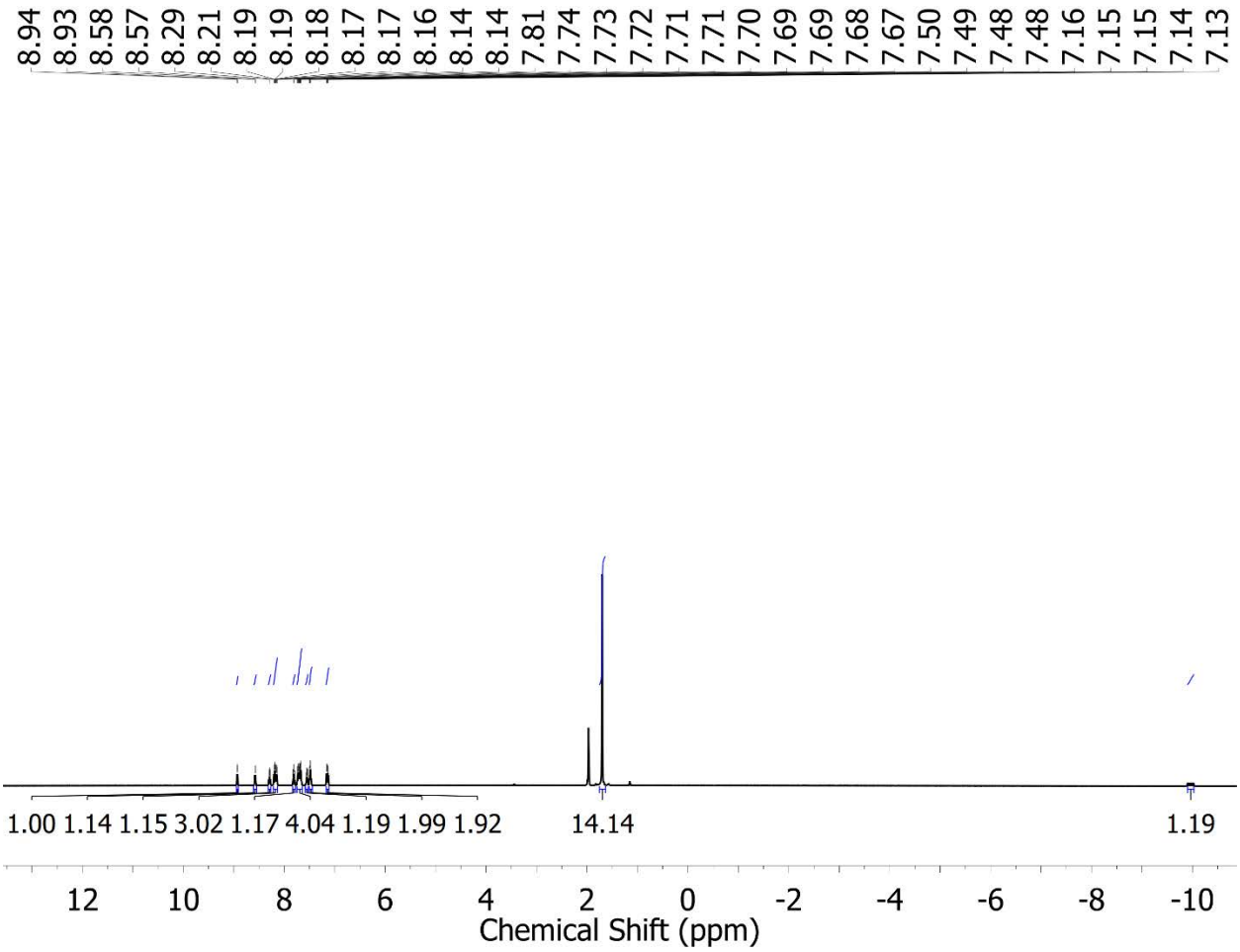

Figure S19. ^{1}H NMR spectrum (400 MHz, CD_3CN) of **3**.

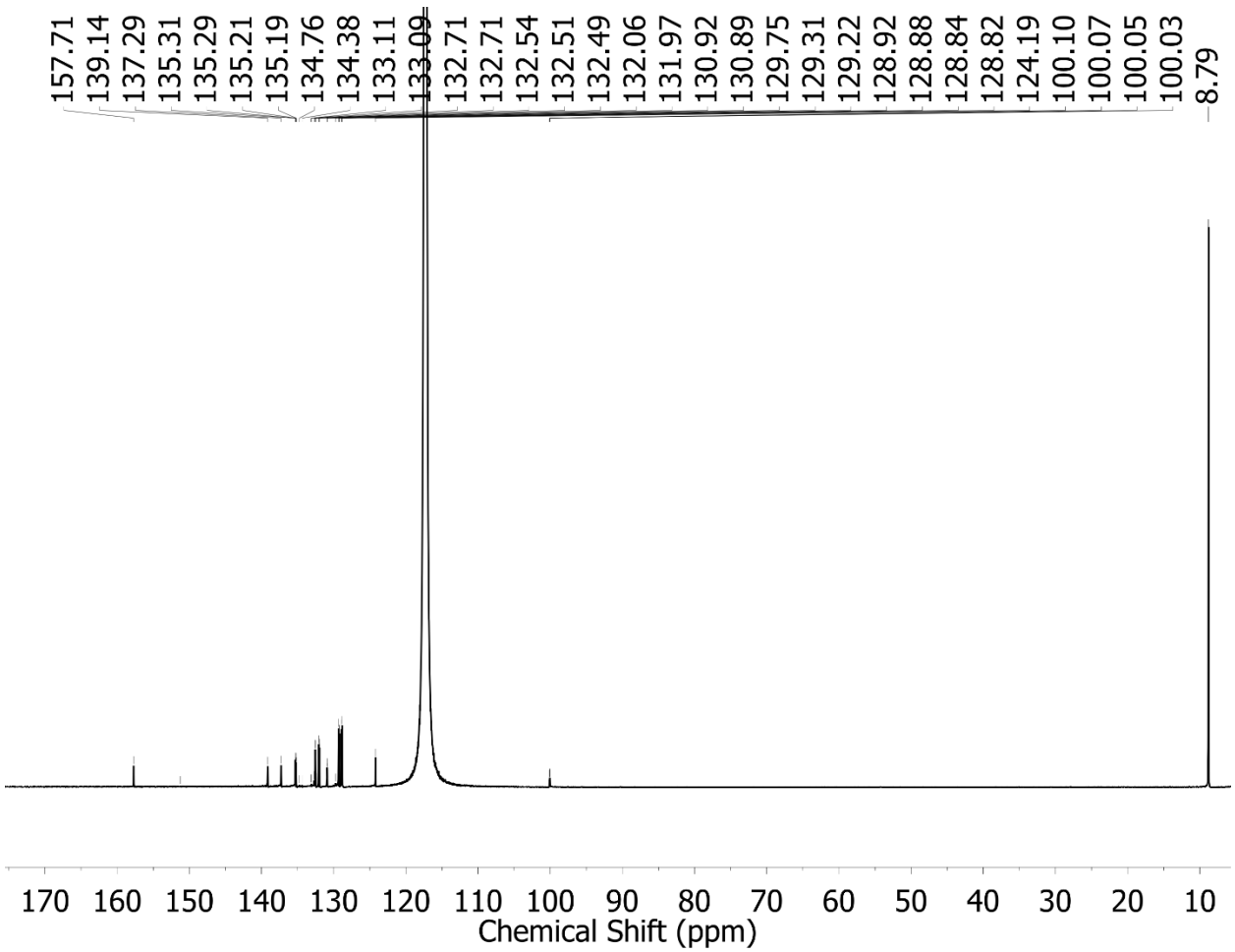

Figure S20. $^{13}C\{^{1}H\}$ NMR spectrum (126 MHz, CD_3CN) of **3**.

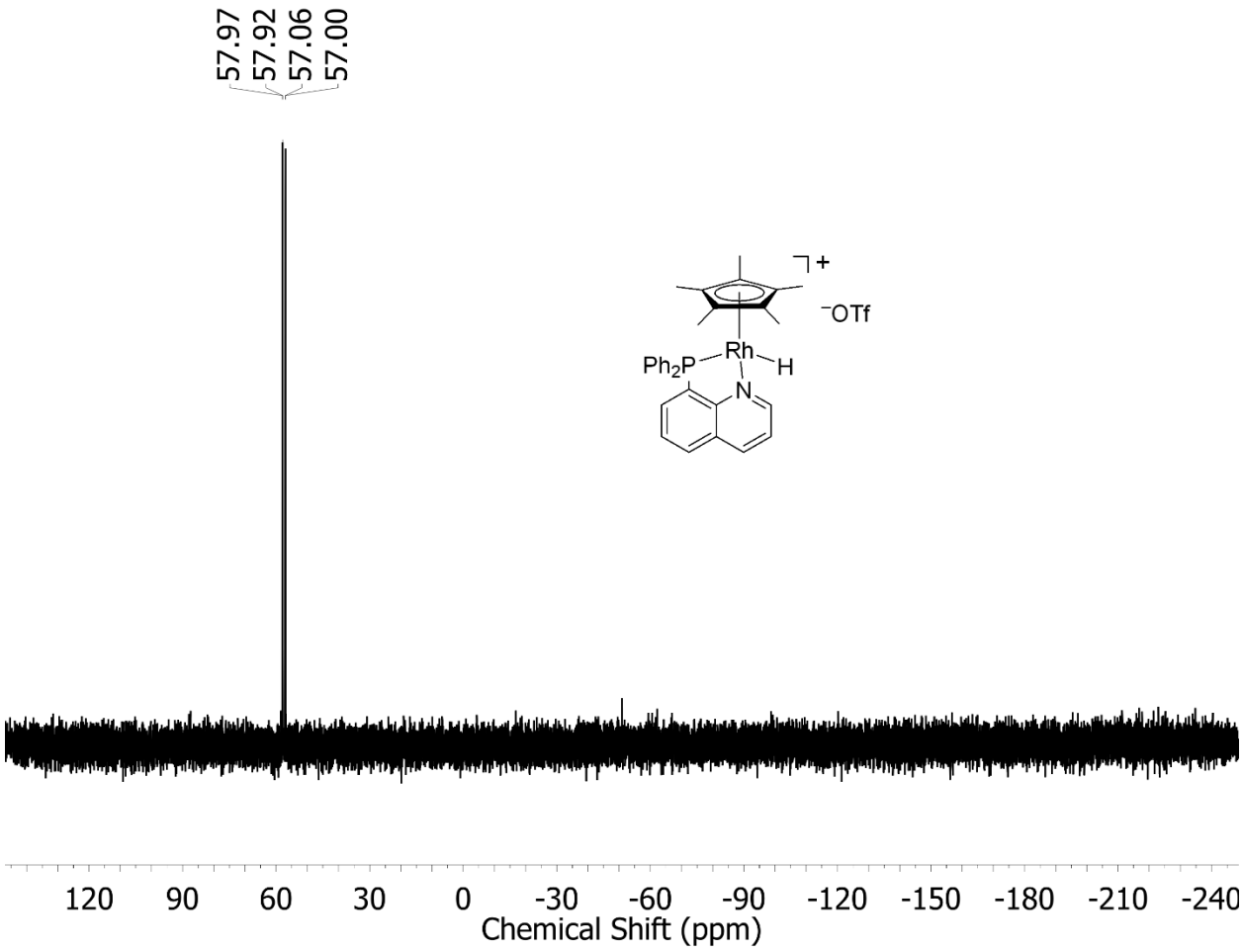

Figure S21. $^{31}P\{^{1}H\}$ NMR spectrum (162 MHz, CD_3CN) of **3**.

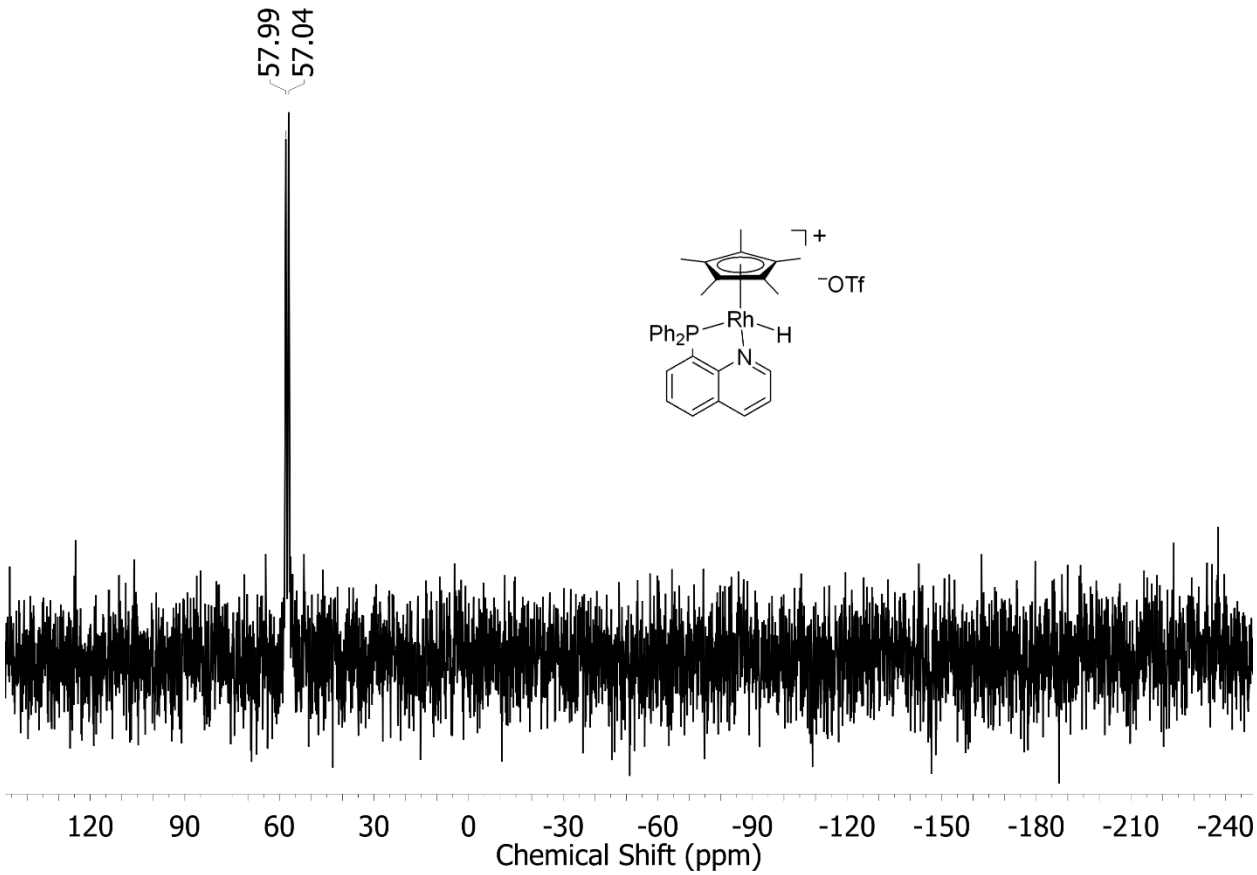

Figure S22. ^{31}P NMR spectrum (162 MHz, CD_3CN) of **3**. $^{2}J_{P,H}$ is not observed, while $^{1}J_{P,Rh}$ of 158 Hz is observed.

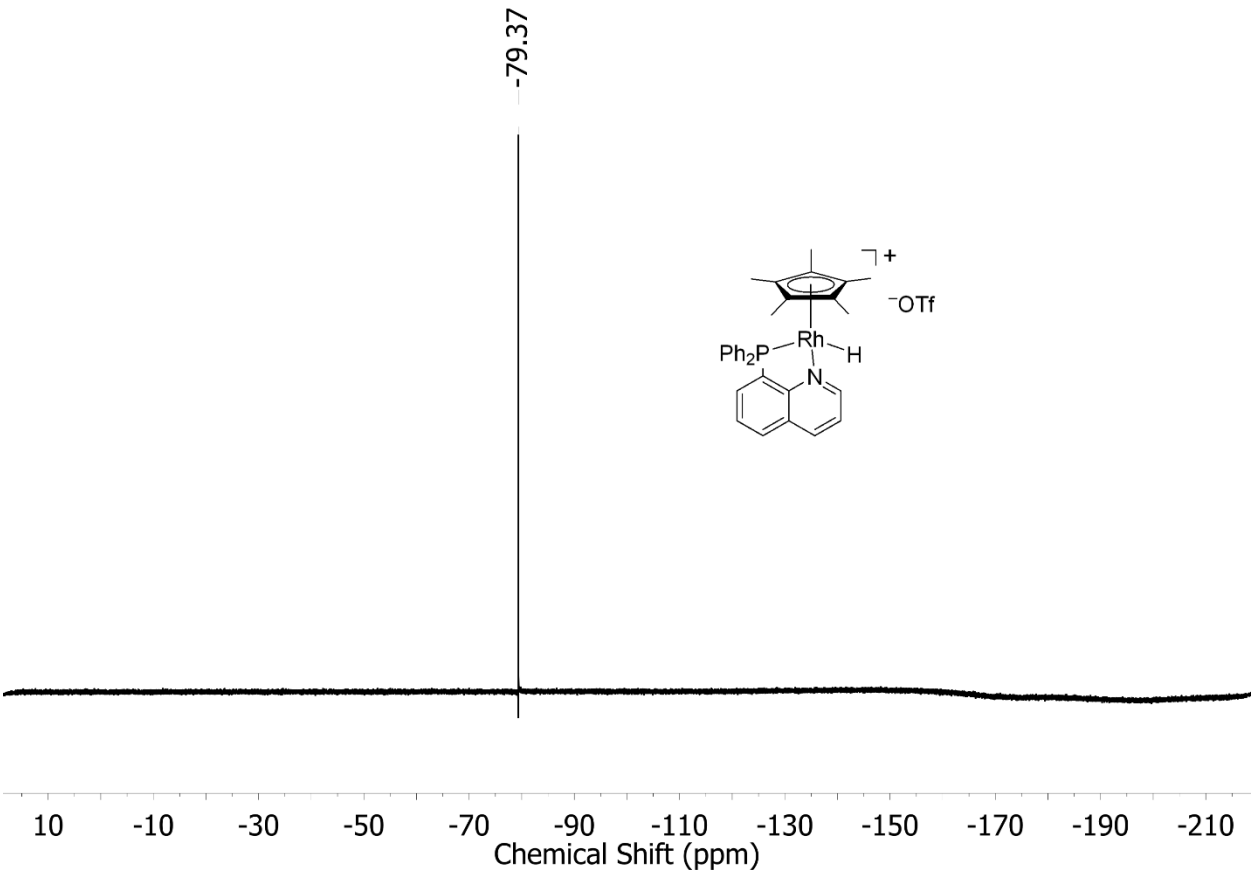

Figure S23. ^{19}F NMR spectrum (376 MHz, CD_3CN) of **3**.

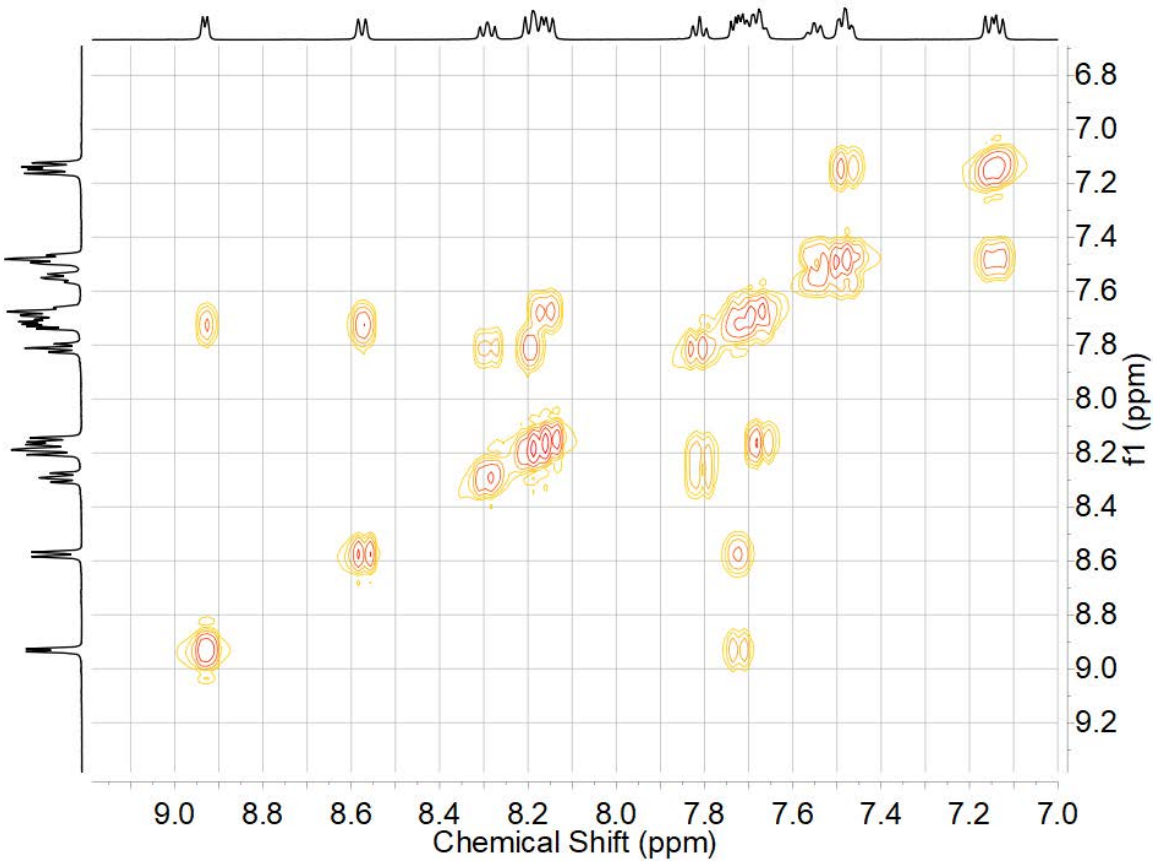

Figure S24. COSY NMR spectrum (CD_3CN) of **3**.

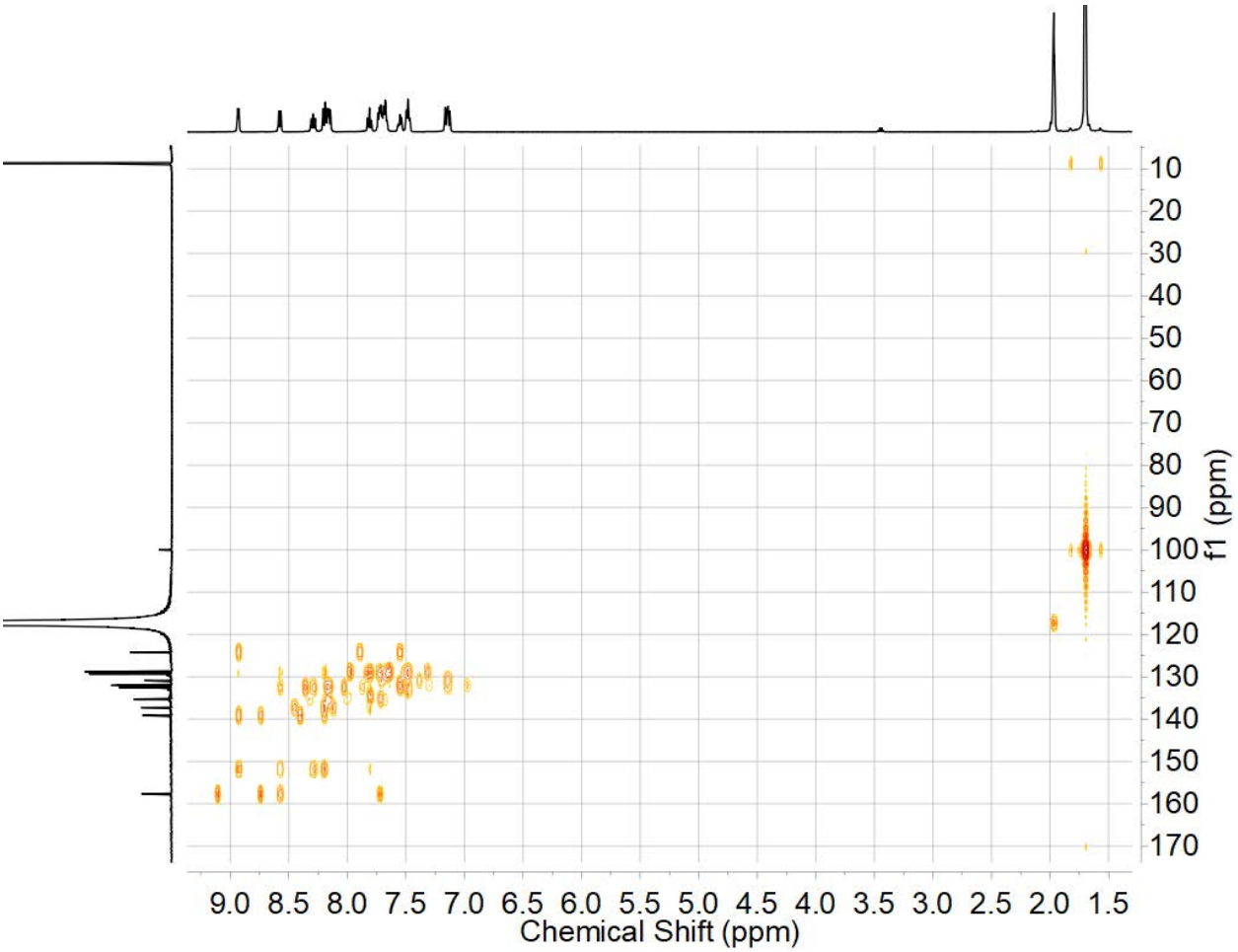

Figure S25. HMBC NMR spectrum (CD_3CN) of **3**.

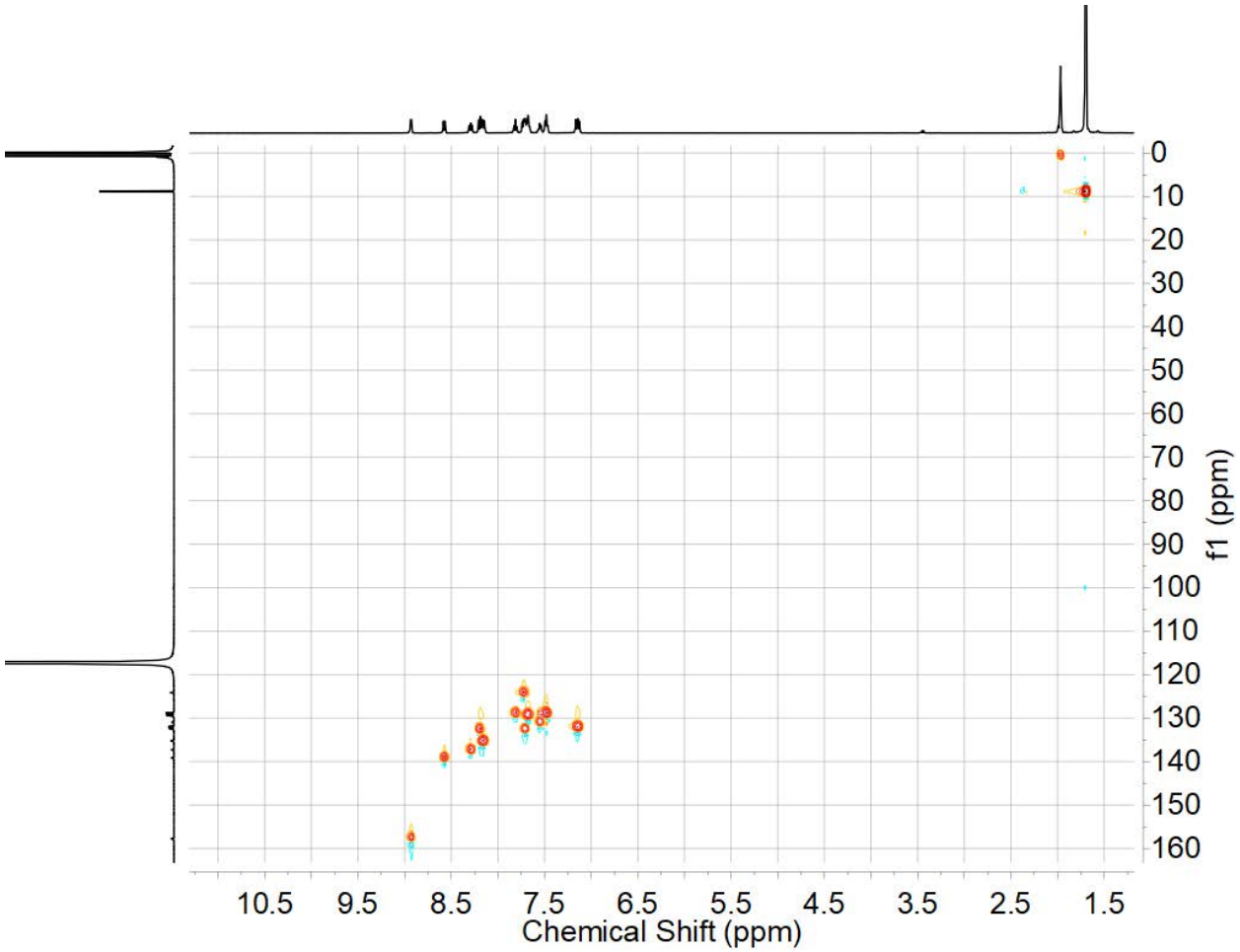

Figure S26. HSQC NMR spectrum (CD_3CN) of **3**.

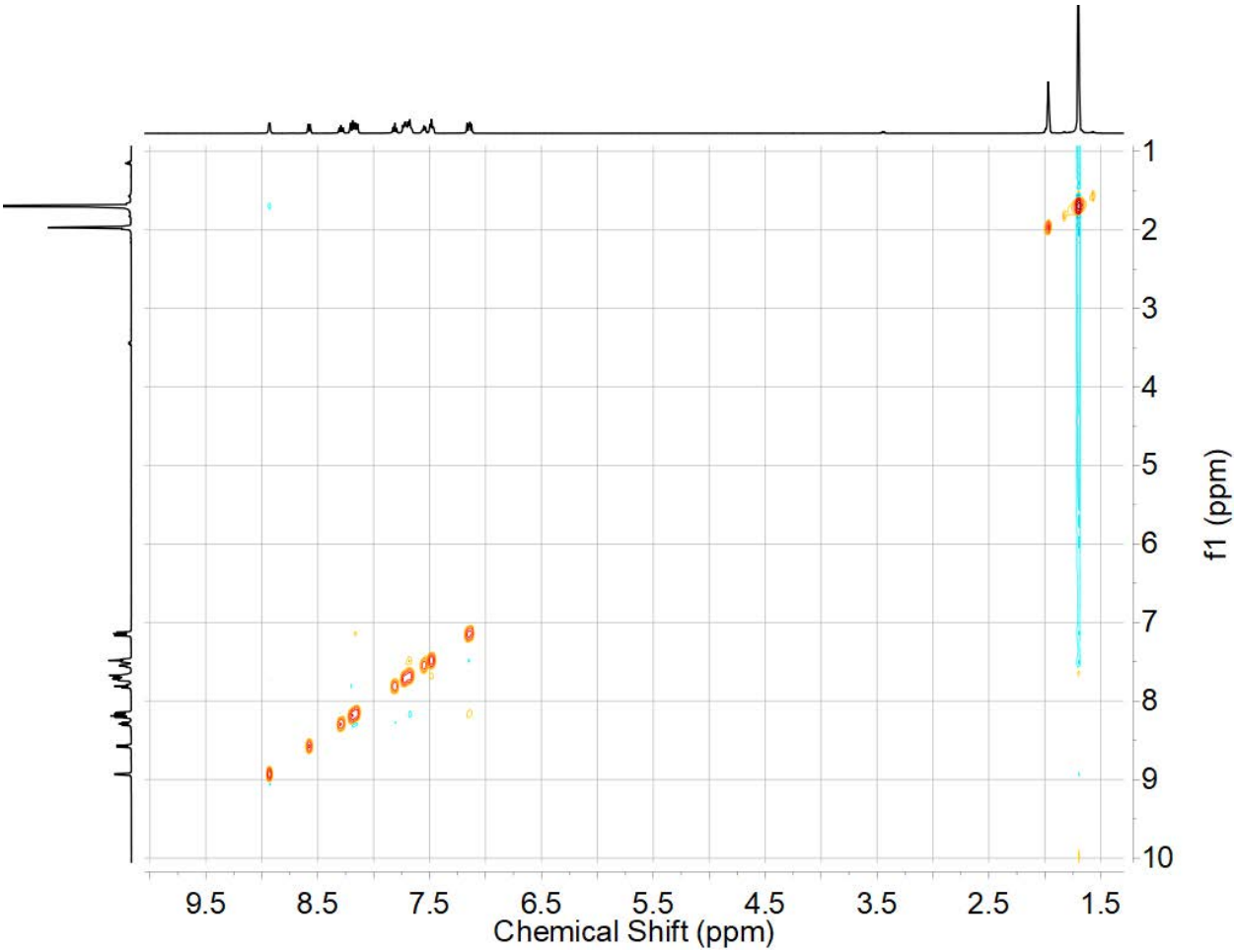

Figure S27. NOESY NMR spectrum (CD_3CN) of **3**.

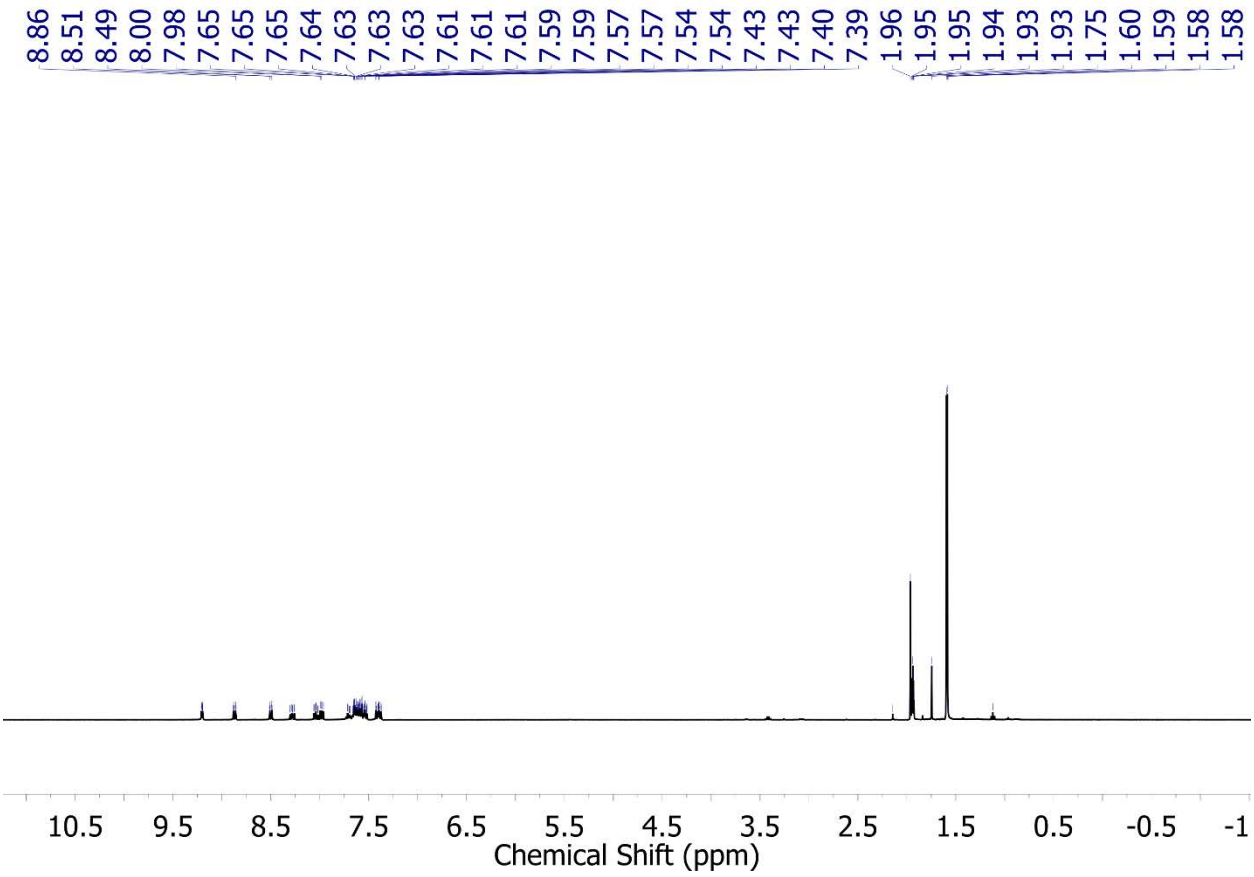

Figure S28. ^{1}H NMR spectrum (400 MHz, CD_3CN) of **1-NCCH$_3$**.

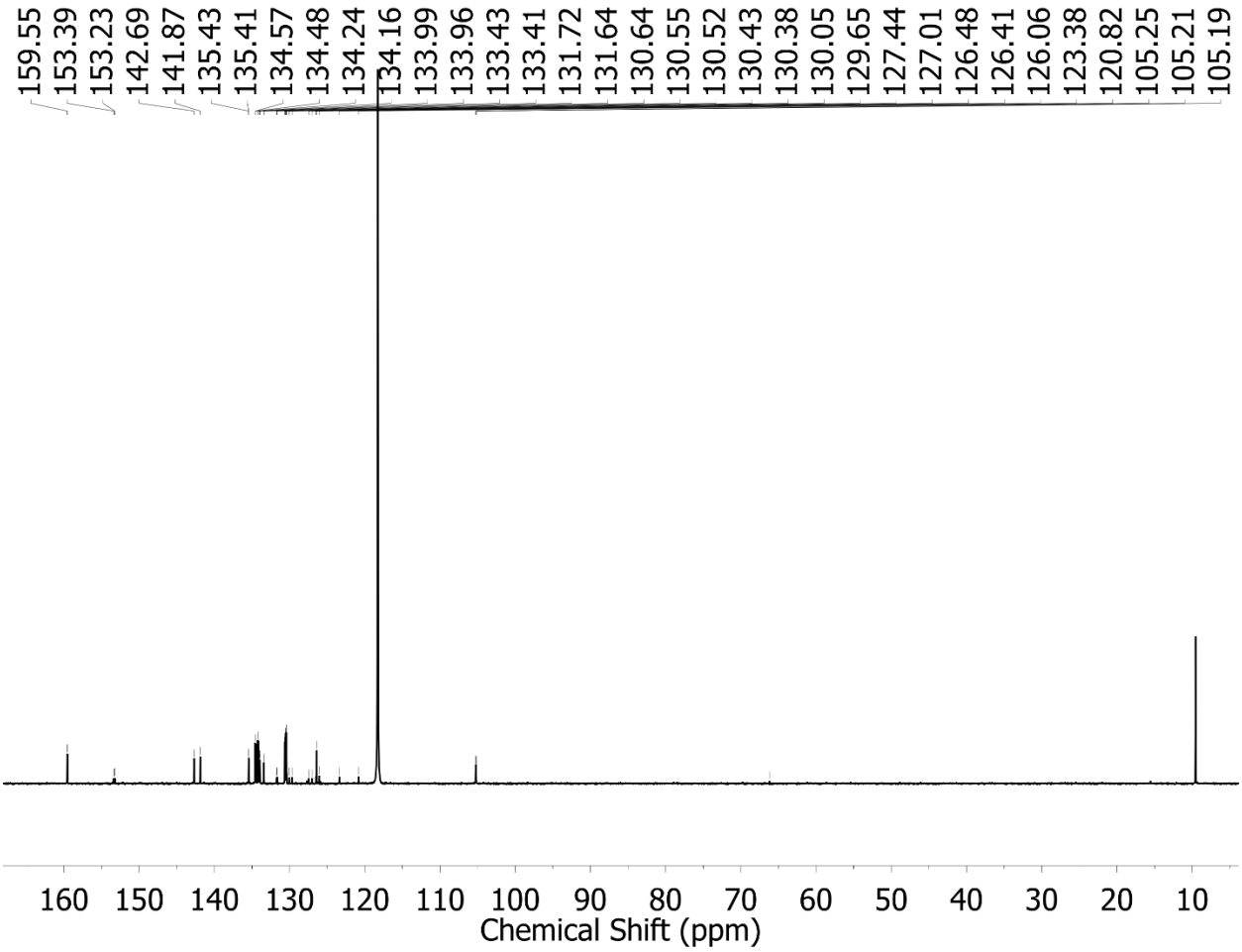

Figure S29. ^{13}C NMR spectrum (162 MHz, CD_3CN) of **1-NCCH$_3$**.

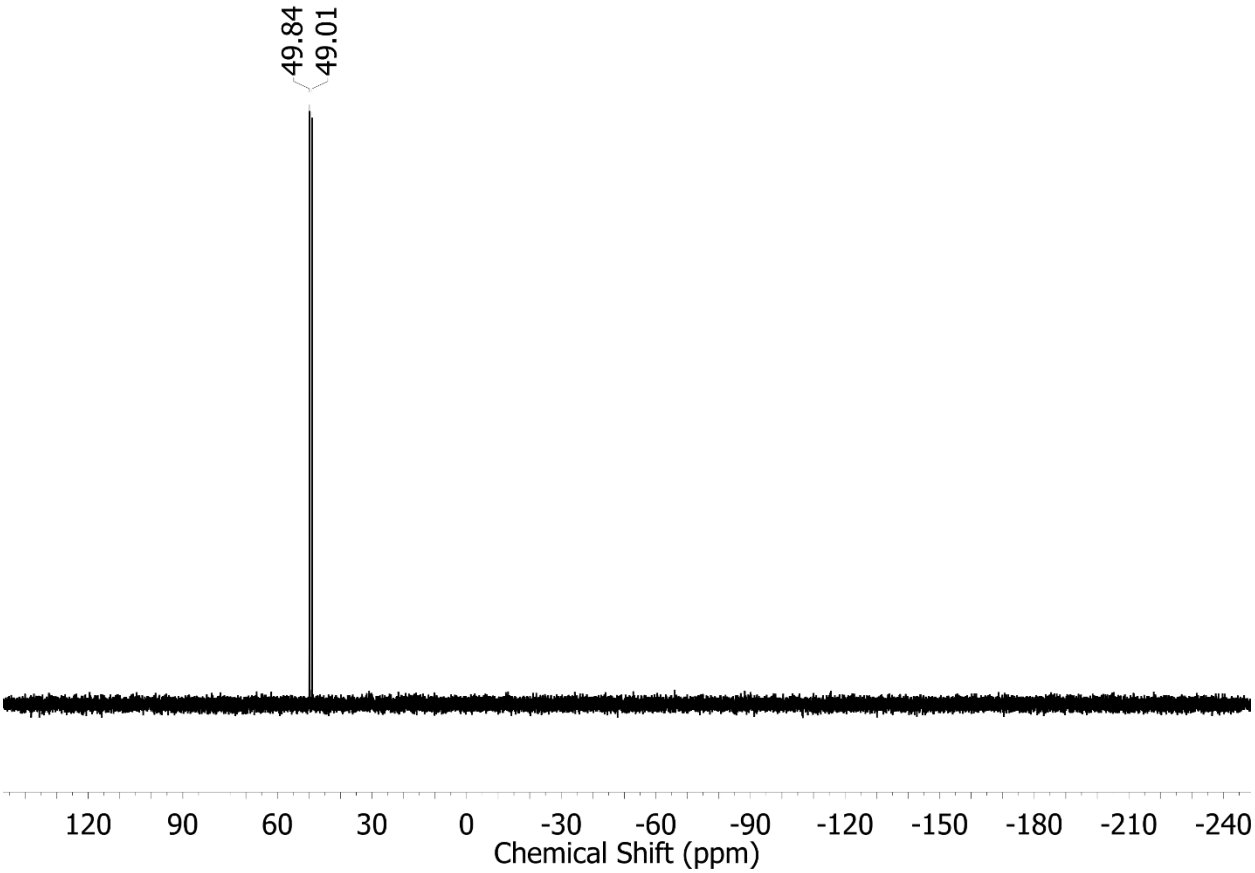

Figure S30. $^{31}P\{^{1}H\}$ NMR spectrum (162 MHz, CD_3CN) of **1-NCCH$_3$**.

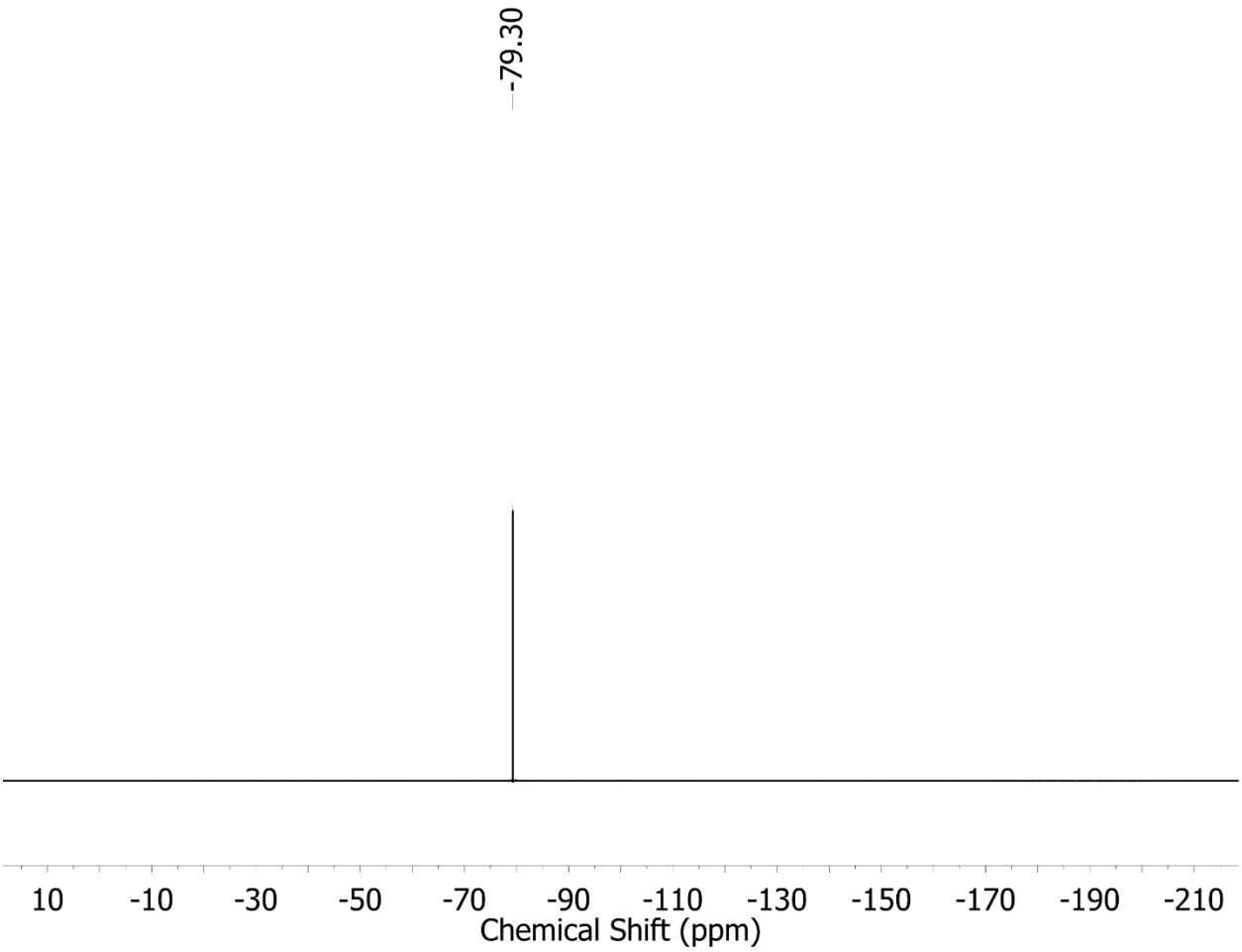

Figure S31. ^{19}F NMR spectrum (162 MHz, CD_3CN) of **1-NCCH$_3$**.

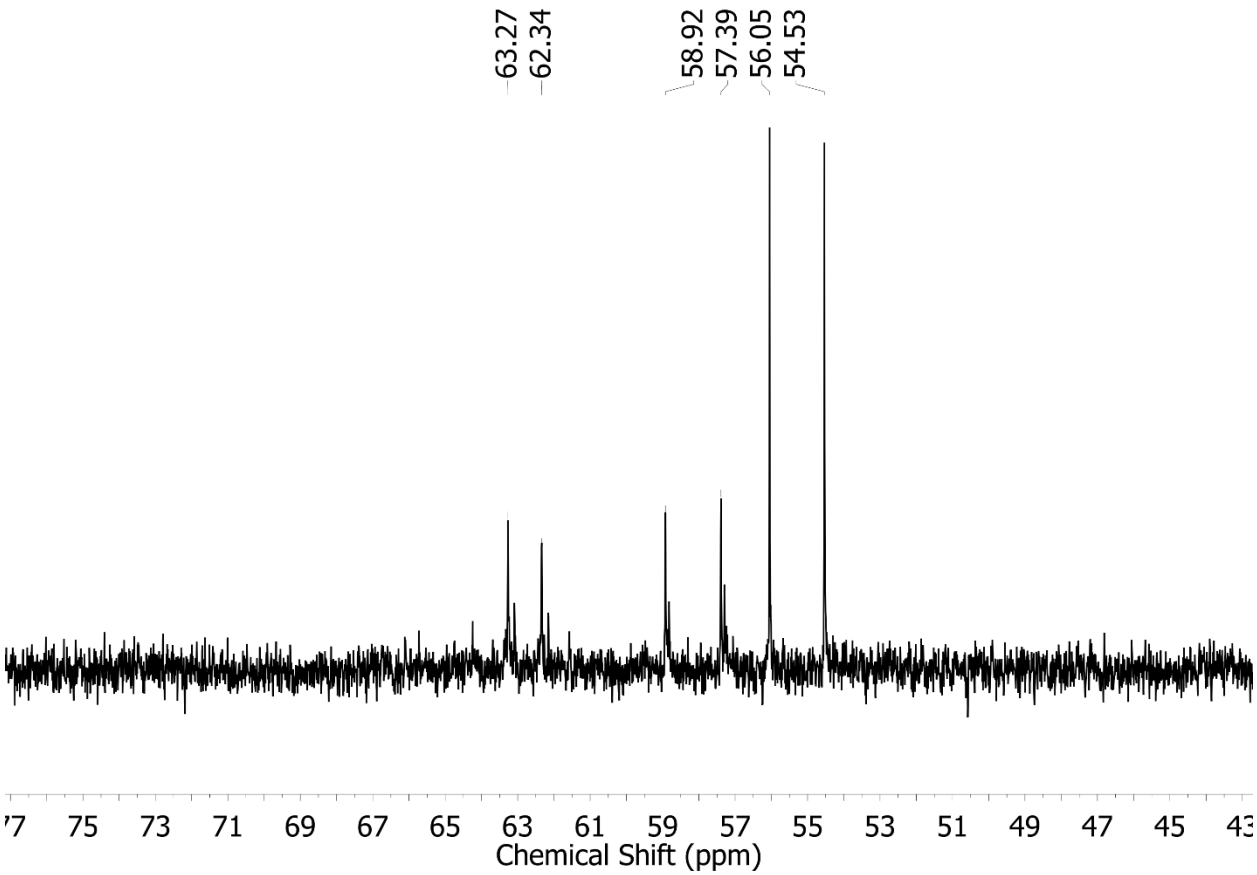

Figure S32. $^{31}P\{^{1}H\}$ NMR spectrum (162 MHz, C_6D_6) of aliquot from chemical reduction of **3** with decamethylcobalacene.

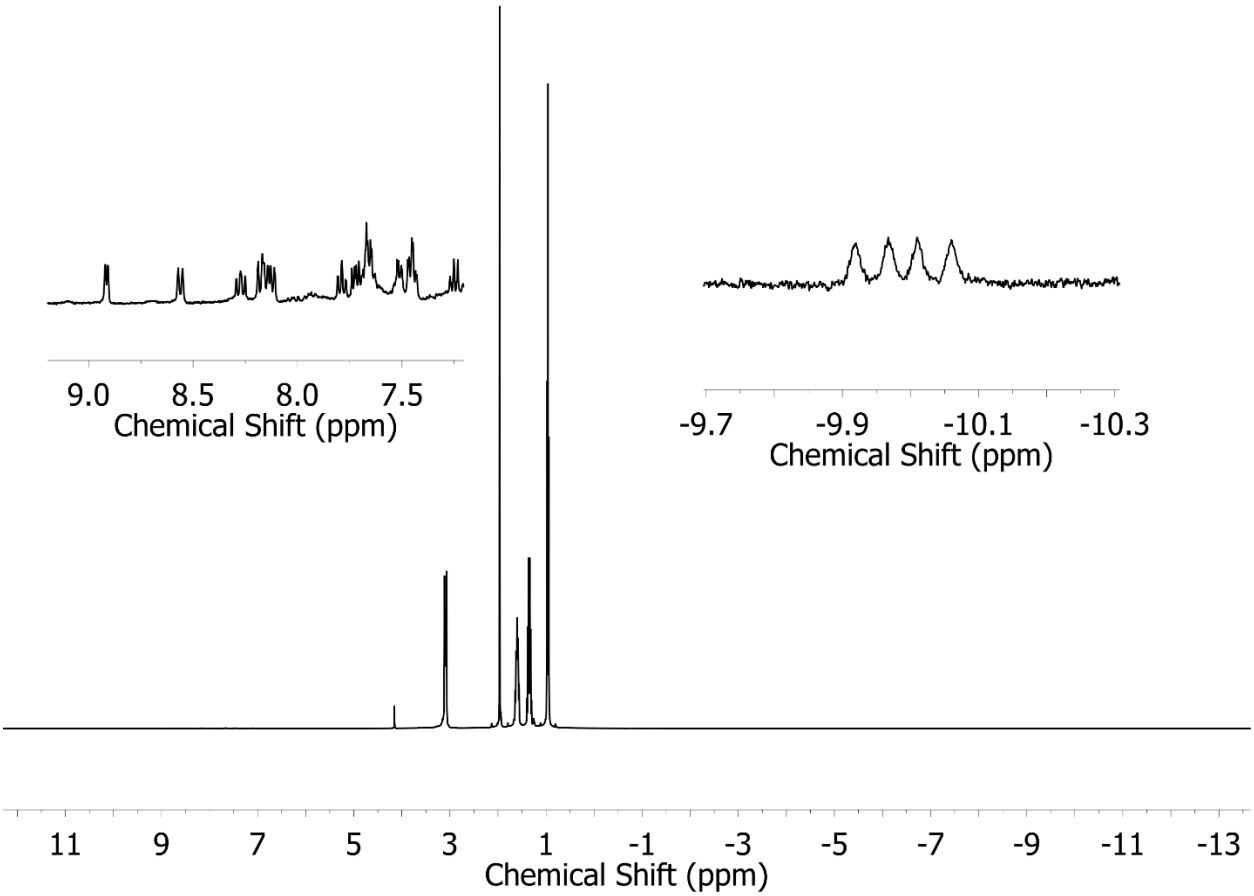

Figure S33. ^{1}H NMR spectrum (162 MHz, CD_3CN) of aliquot from bulk electrolysis of **1-NCCH$_3$** with 10 equiv. of $Et_3NH^+OTf^-$.

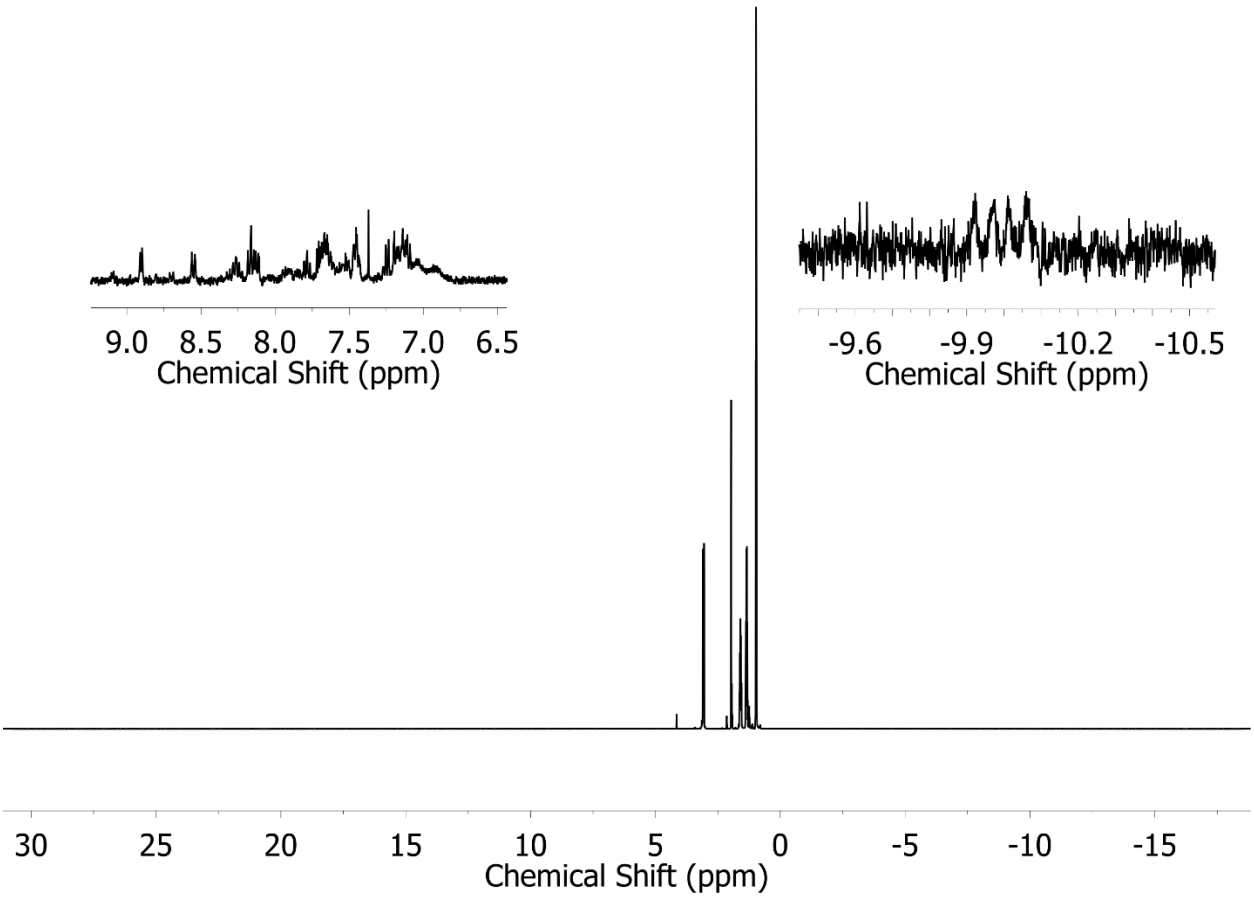

Figure S34. ^{1}H NMR spectrum (162 MHz, CD_3CN) of aliquot from bulk electrolysis of **1- Cl** with 10 equiv. of $Et_3NH^{+}OTf^{-}$.

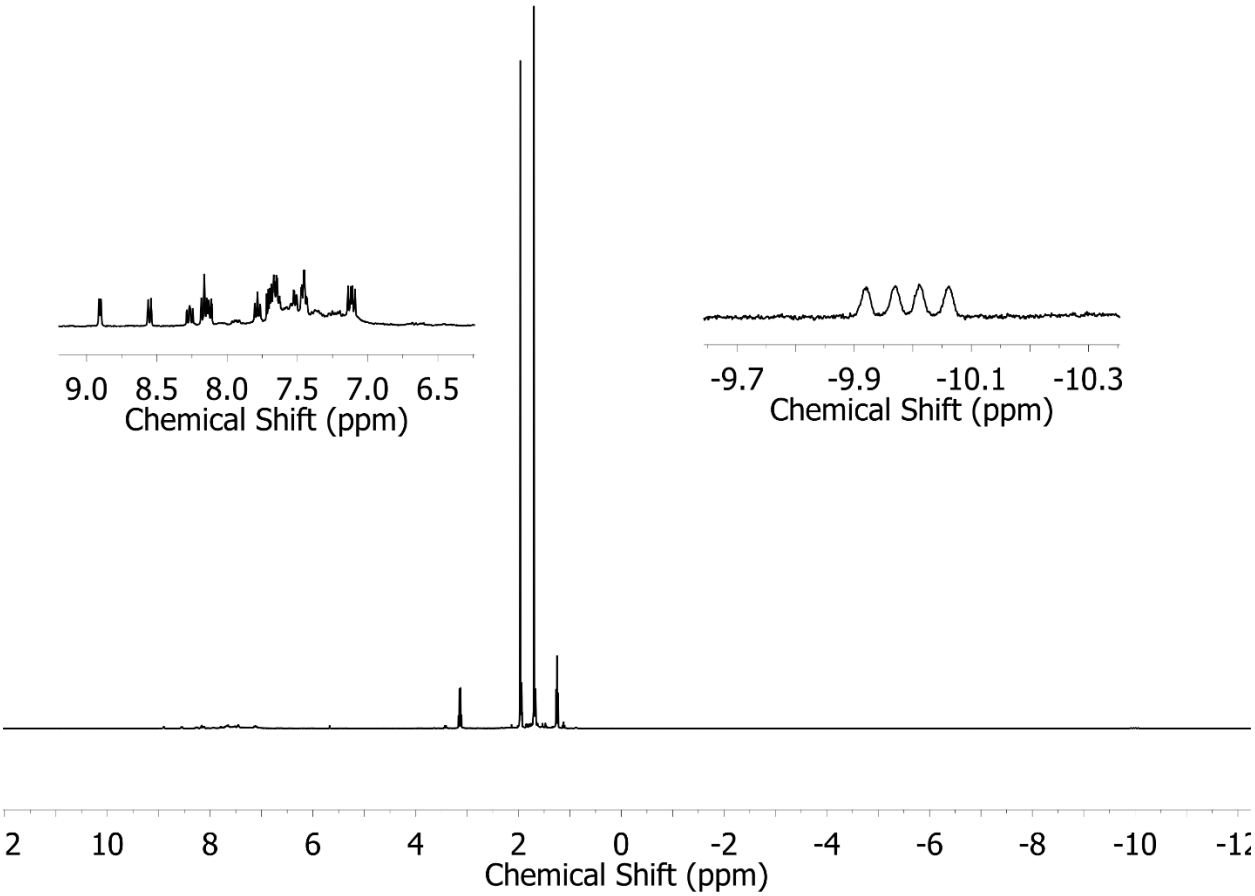

Figure S35. ^{1}H NMR spectrum (162 MHz, CD_3CN) of aliquot from chemical reduction of **3** with 1 equiv. of $Et_3NH^{+}OTf^{-}$ and decamethylcobaltacene.

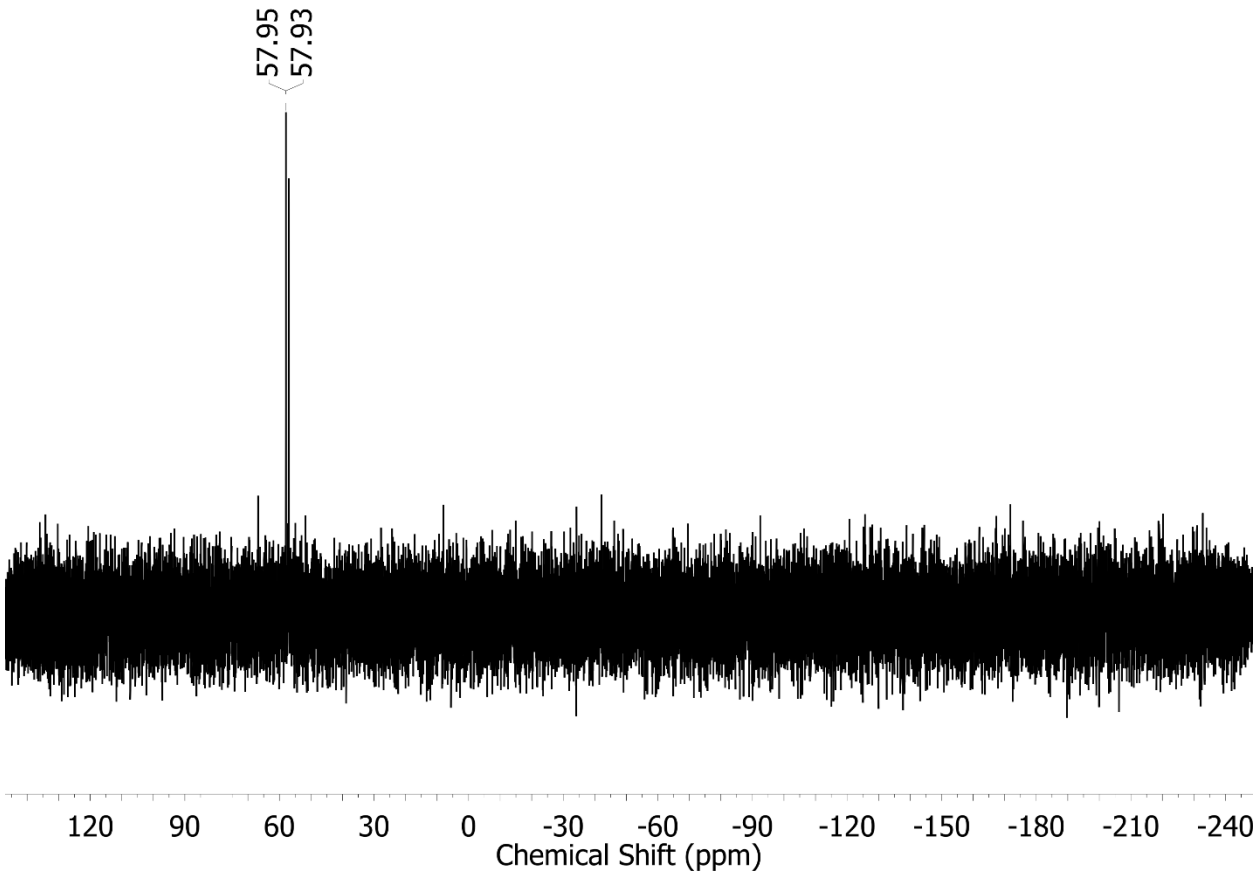

Figure S36. $^{31}P\{^{1}H\}$ NMR spectrum (162 MHz, CD_3CN) of aliquot from chemical reduction of **3** with 1 equiv. of $Et_3NH^+OTf^-$ and decamethylcobaltacene.

UV-Vis

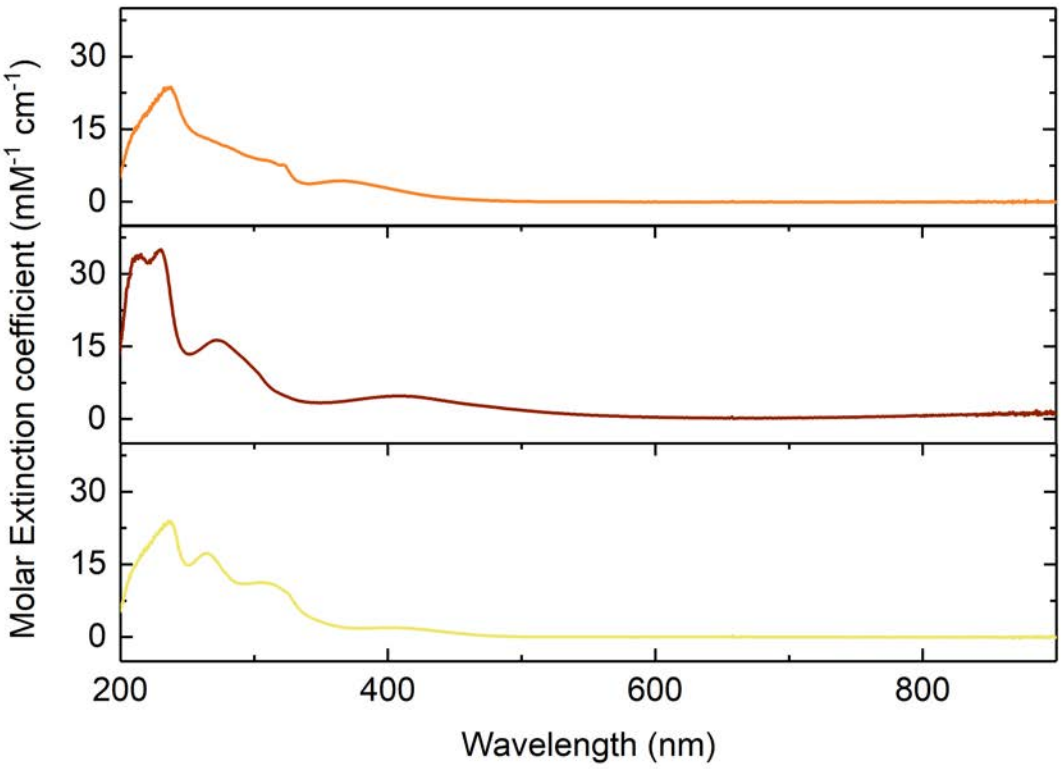

Figure S37. Electronic absorption spectra of **1-Cl** (upper panel), **2** (middle panel), and **3** (lower panel) in CH_3CN.

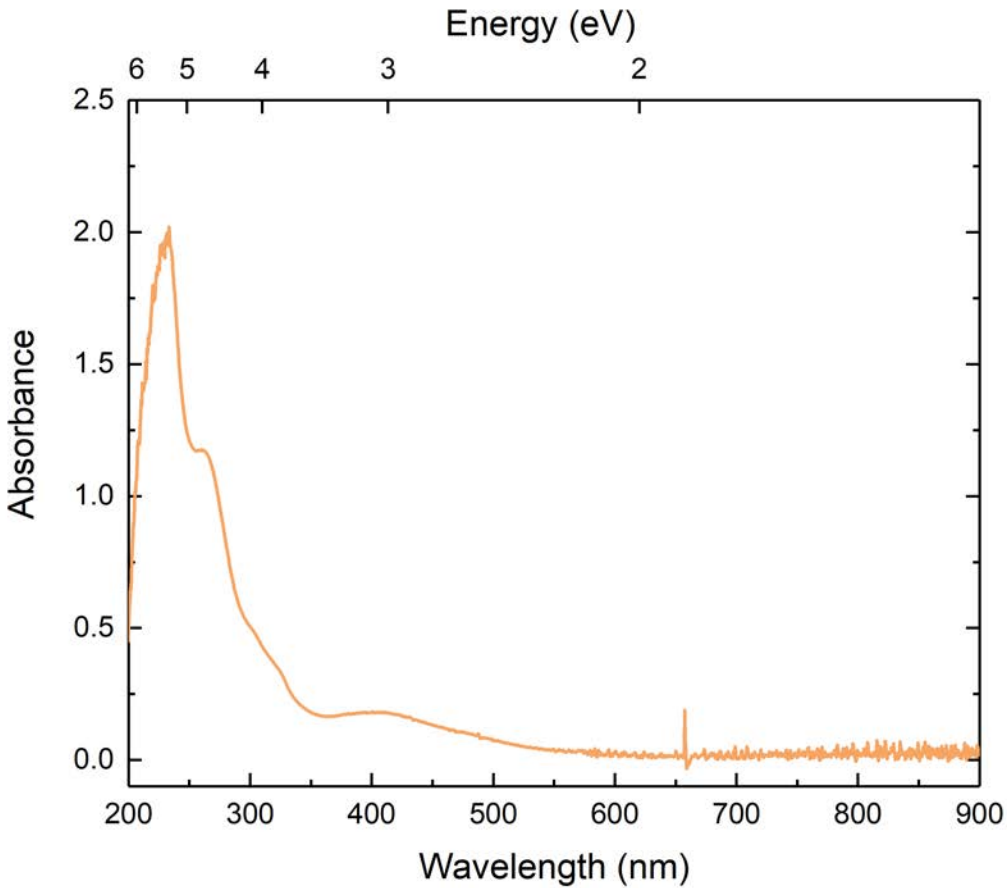

Figure S38. Electronic absorption spectrum of aliquot (CH_3CN) from bulk electrolysis of **3**.

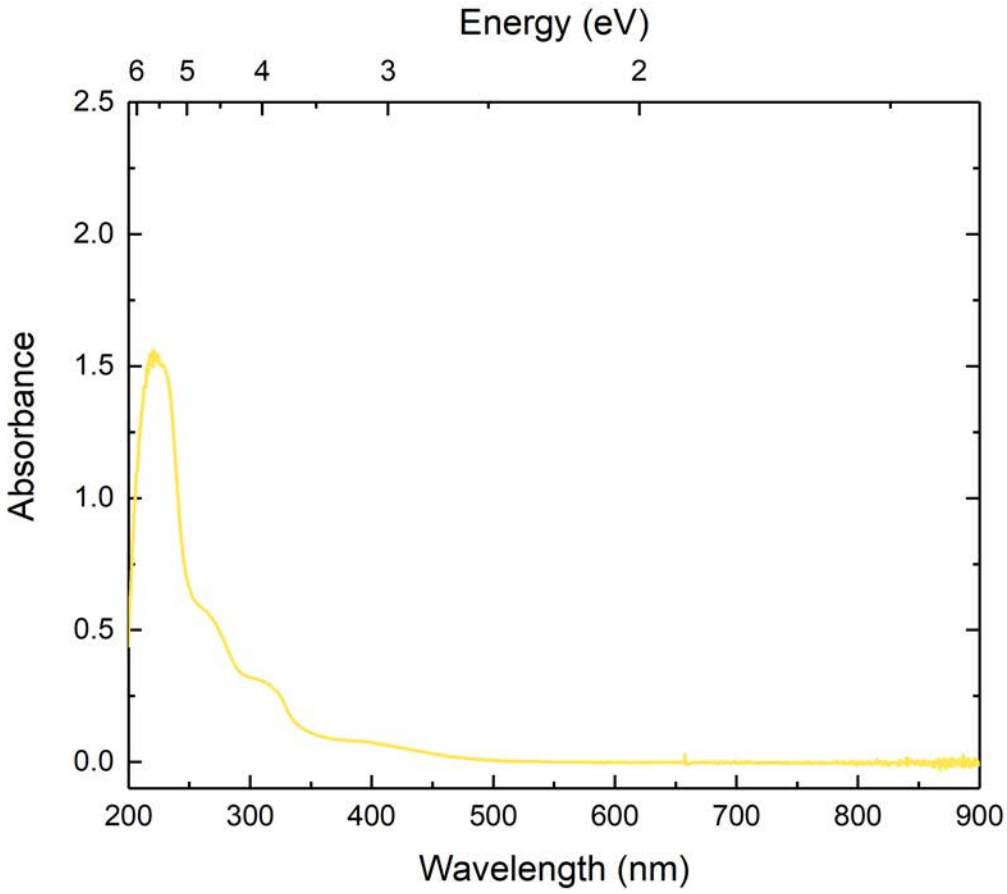

Figure S39. Electronic absorption spectrum of aliquot (CH_3CN) from bulk electrolysis of for **1-NCCH$_3$** with 10 equiv. of $Et_3NH^+OTf^-$.

Electrochemistry

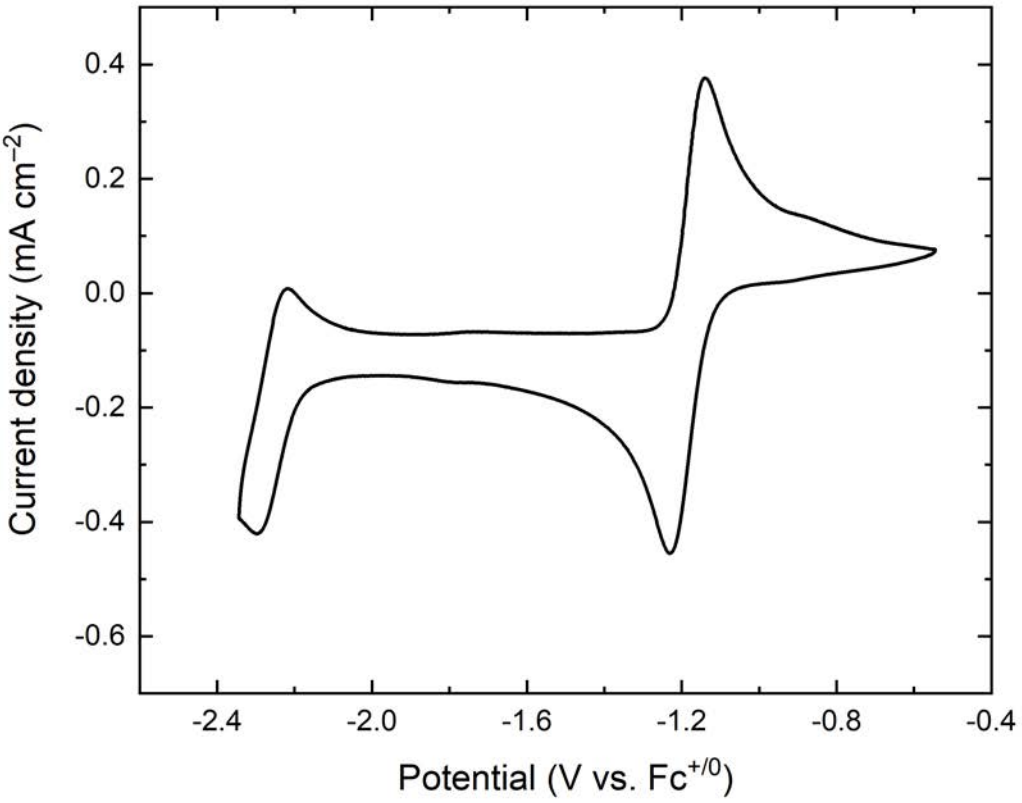

Figure S40. Cyclic voltammetry of **1-Cl** (CH_3CN, 0.1 M [$^nBu_4N$][PF_6], 100 mV/s)

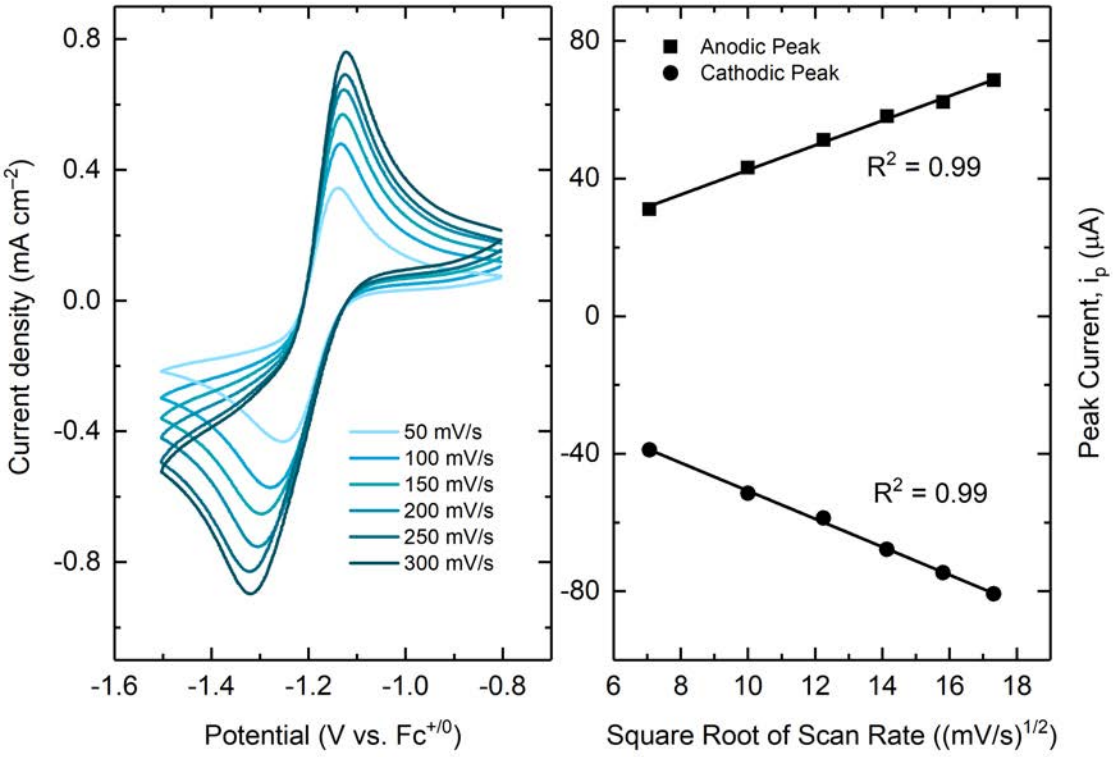

Figure S41. Left: cyclic voltammetry of first reduction event **1-Cl** at varying scan rate in CH_3CN (0.1 M [^{n}Bu$_4$N][PF$_6$]). Right: linear dependence of peak cathodic current on square root of scan rate with the y-intercept set to 0.

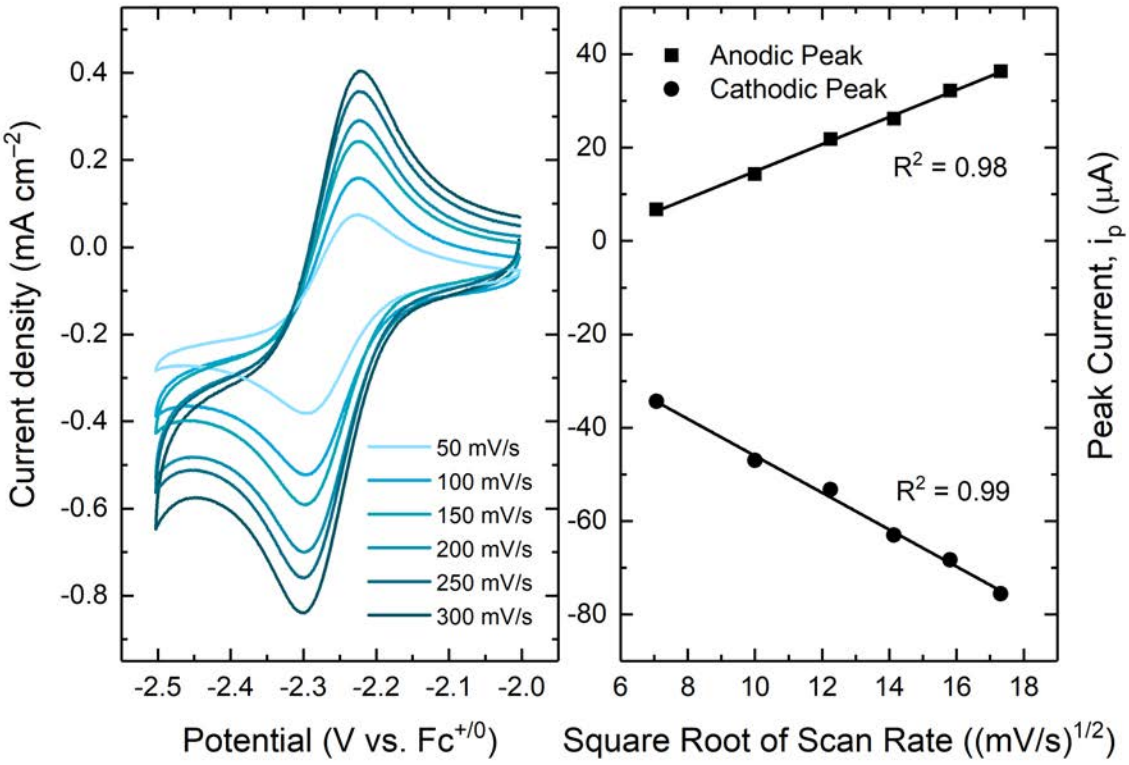

Figure S42. Left: cyclic voltammetry of second reduction event **1-Cl** at varying scan rate in CH_3CN (0.1 M [^{n}Bu$_4$N][PF$_6$]). Right: linear dependence of peak cathodic current on square root of scan rate.

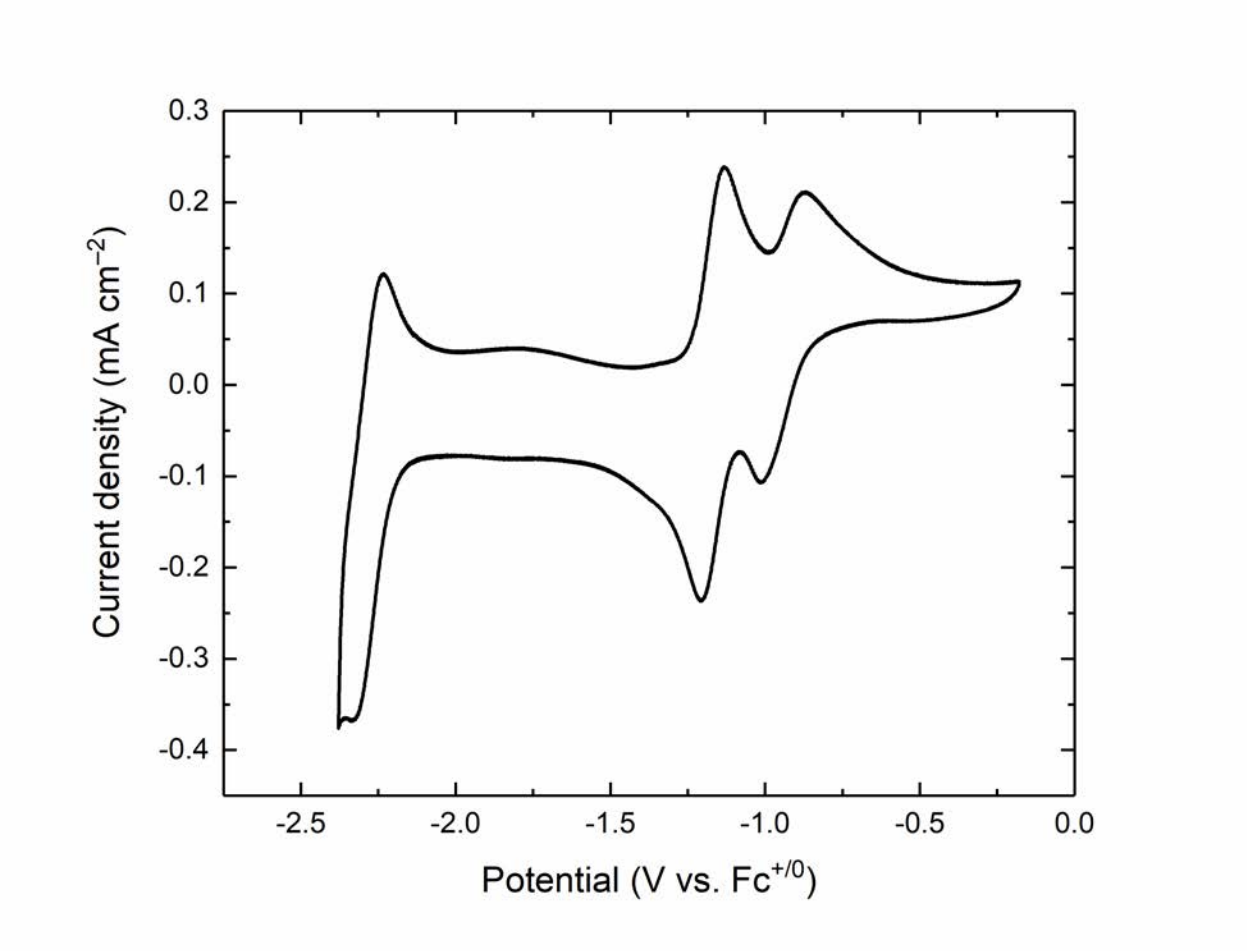

Figure S43. Cyclic voltammetry of **1-NCCH$_3$** (CH_3CN, 0.1 M [$^nBu_4N$][PF_6], 100 mV/s).

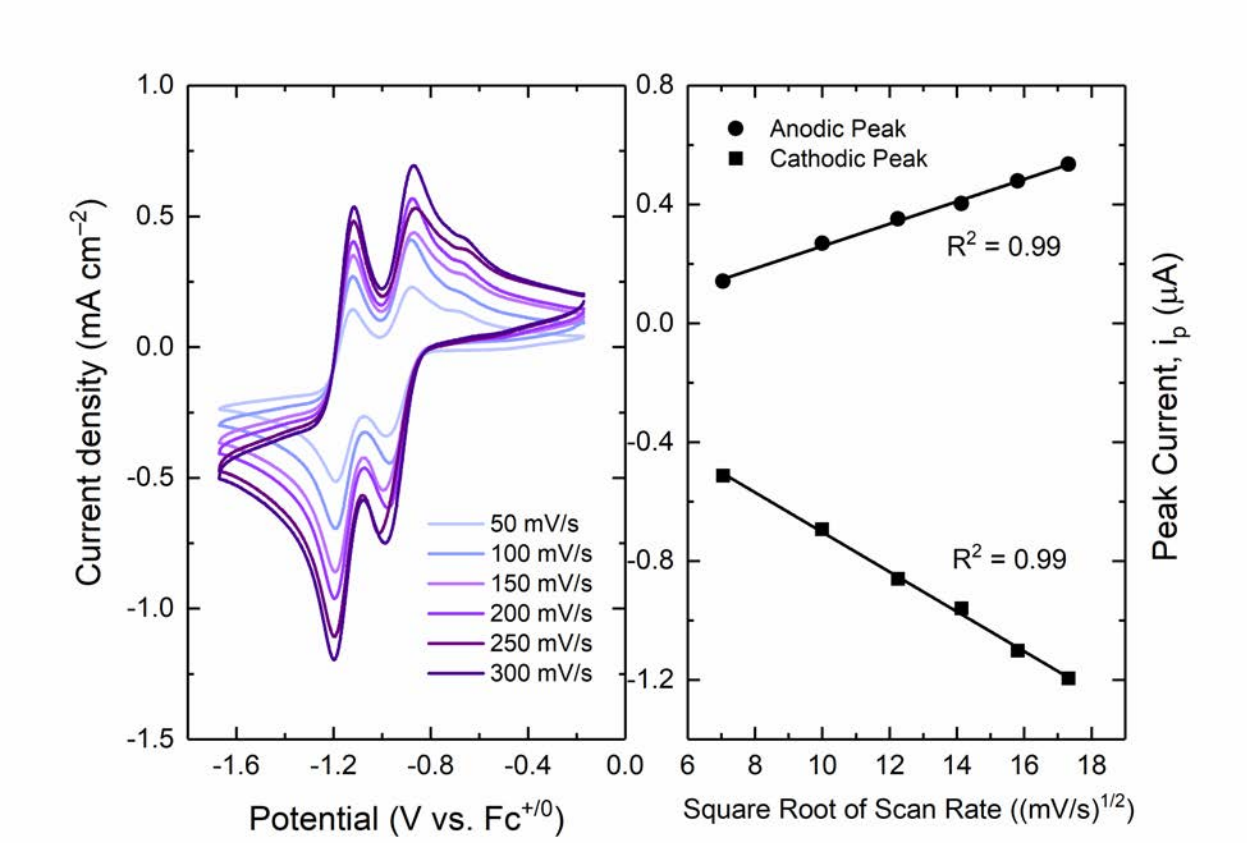

Figure S44. Left: cyclic voltammetry of second reduction event **1-NCCH$_3$** at varying scan rate in CH_3CN (0.1 M [^{n}Bu$_4$N][PF$_6$]). Right: linear dependence of peak cathodic current on square root of scan rate.

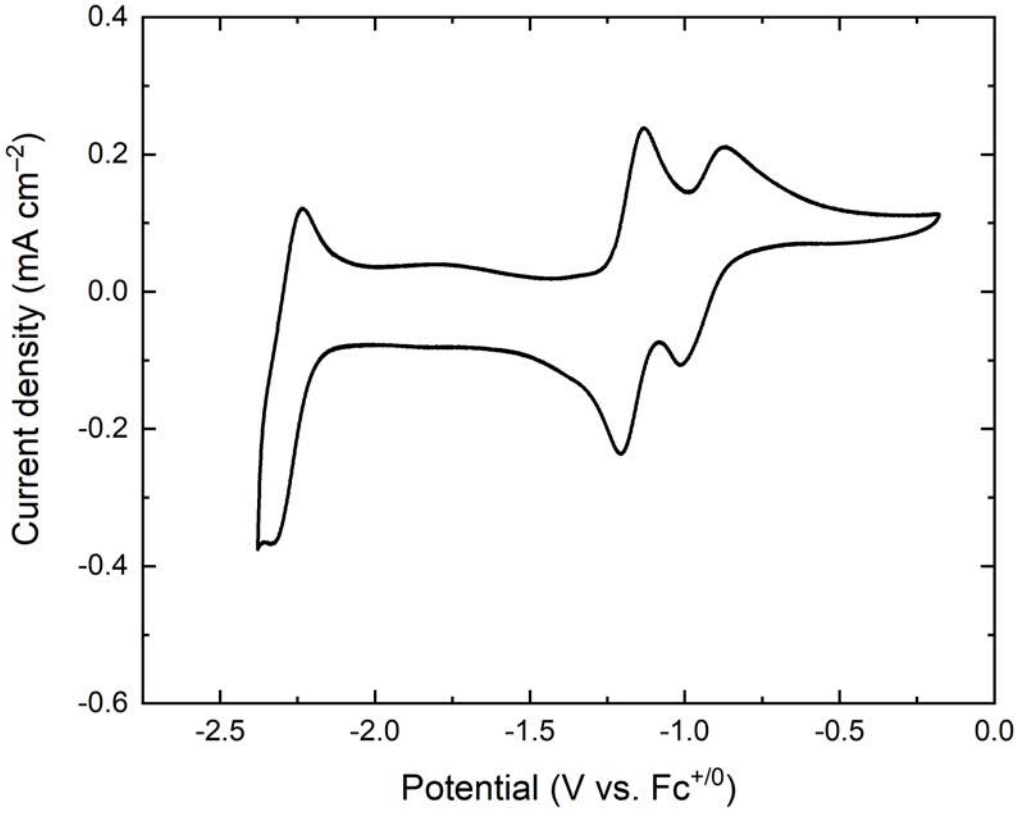

Figure S45. Cyclic voltammetry of **2** (CH_3CN, 0.1 M [$^nBu_4N$][PF_6], 100 mV/s)

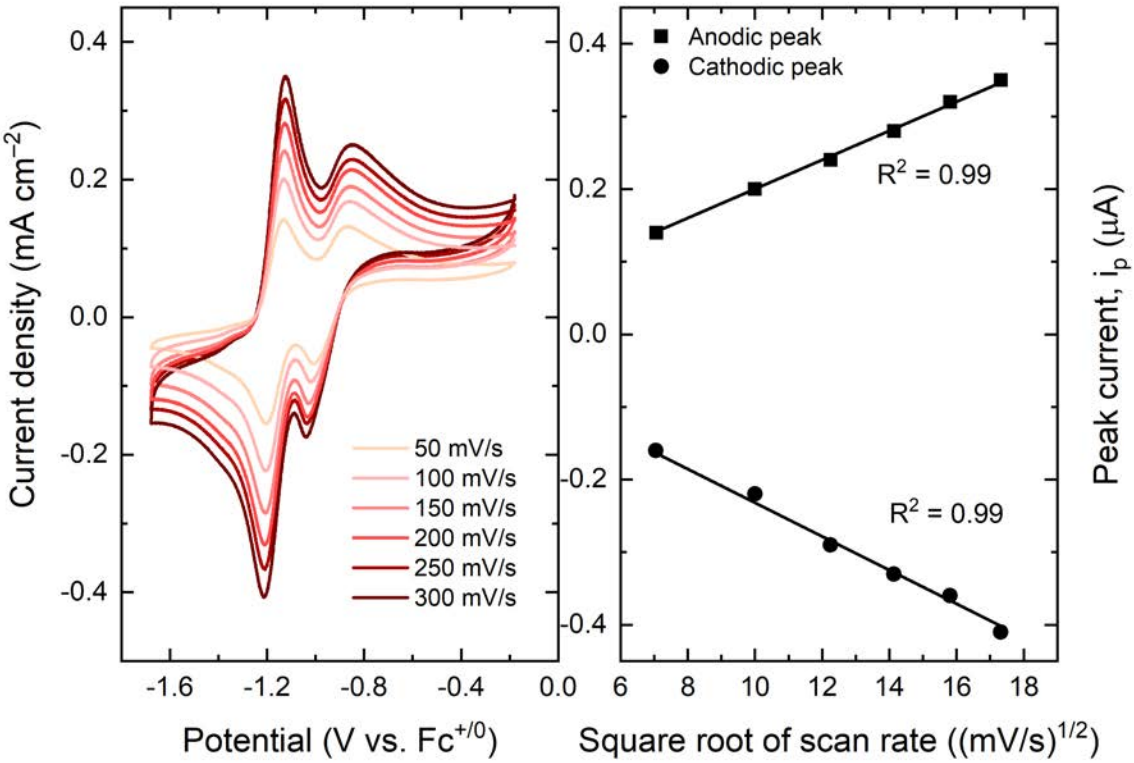

Figure S46. Left: cyclic voltammetry of **2** at varying scan rate in CH_3CN (0.1 M [^{n}Bu$_4$N][PF_6]). Right: linear dependence of peak cathodic current on square root of scan rate with the y-intercept set to 0.

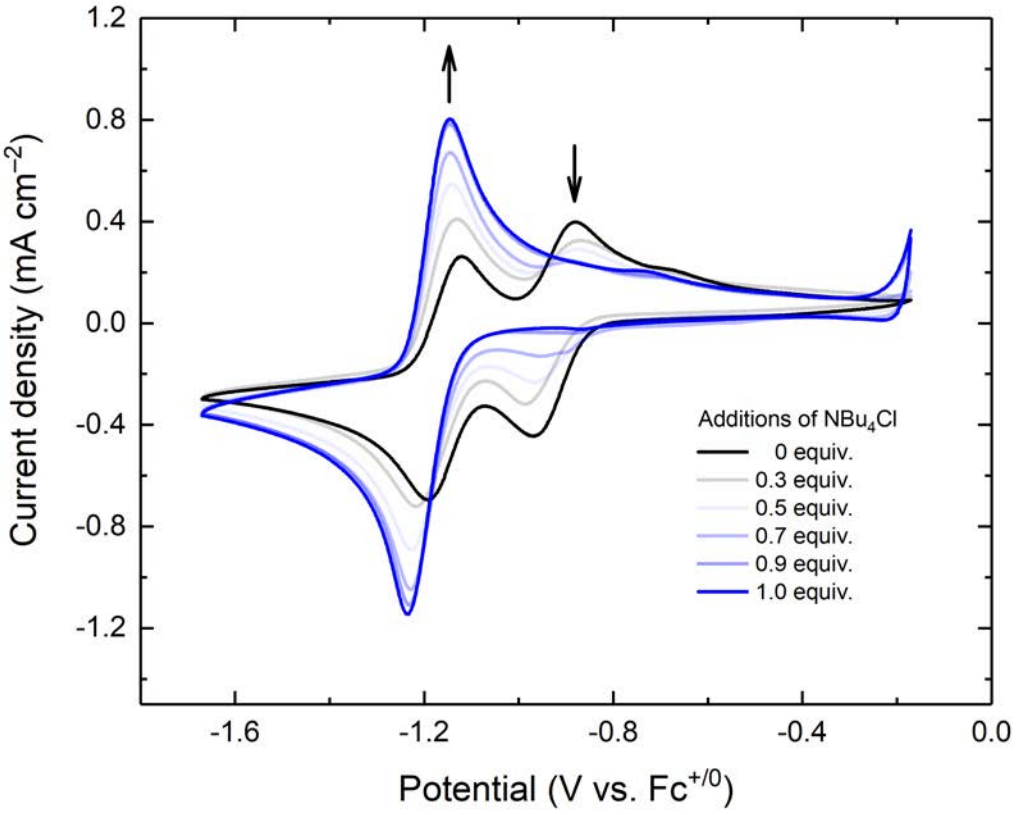

Figure S47. Titration of **1-NCCH$_3$** [^{n}Bu$_4$N][PF$_6$] solution with increasing equivalents of [^{n}Bu$_4$N][Cl] (CH$_3$CN, 0.1 M [^{n}Bu$_4$N][PF$_6$], 100 mV/s).

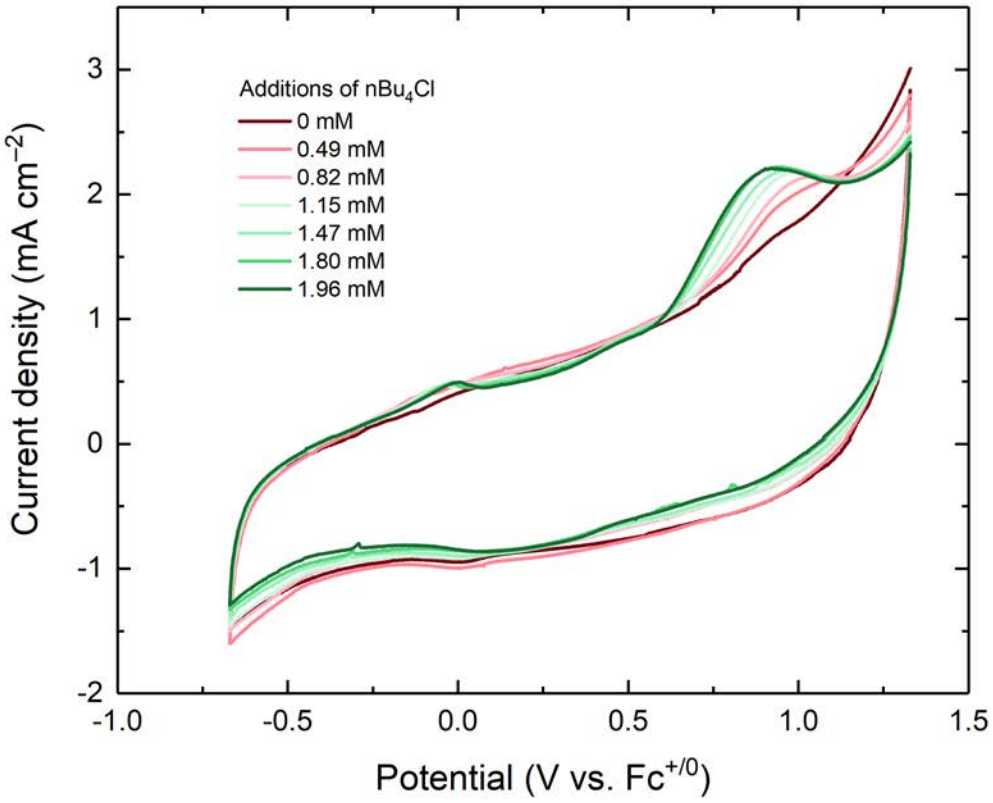

Figure S48. Titration of blank 0.1M [^{n}Bu$_4$N][PF$_6$] solution with increasing equivalents of [^{n}Bu$_4$N][Cl] (CH$_3$CN, 0.1 M [^{n}Bu$_4$N][PF$_6$], 100 mV/s).

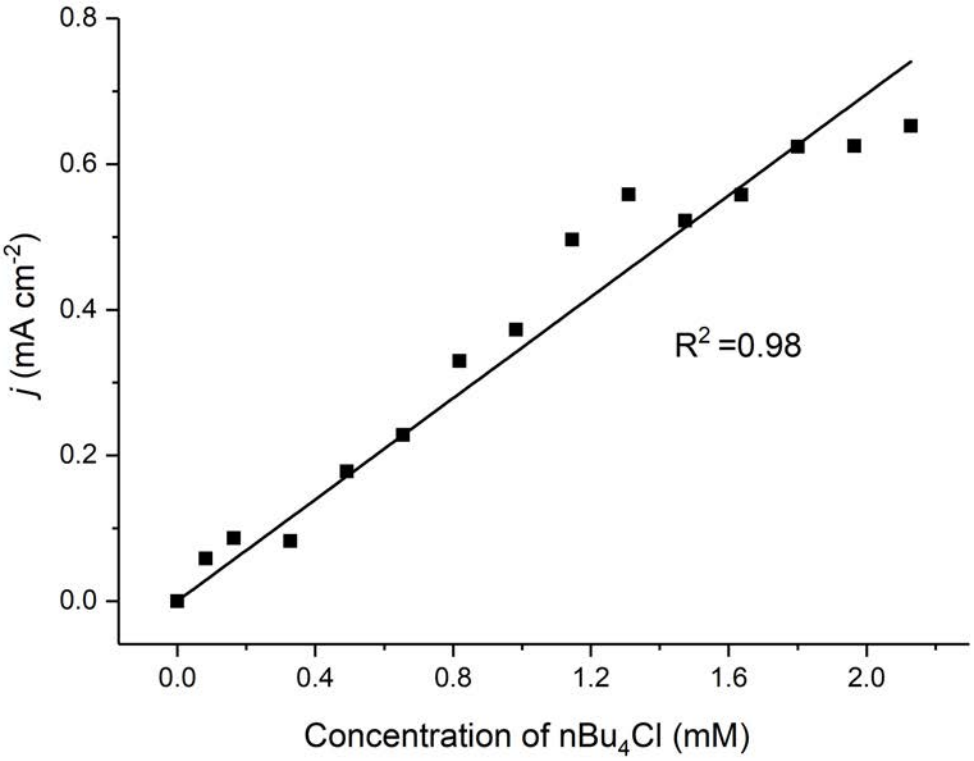

Figure S49. Linear regression of i_{pa} vs. concentration of [^{n}Bu$_4$N][Cl]. Titration of blank 0.1M [^{n}Bu$_4$N][PF_6] solution with increasing equivalents of [^{n}Bu$_4$N][Cl] (CH_3CN, 0.1 M [^{n}Bu$_4$N][PF_6], 100 mV/s).

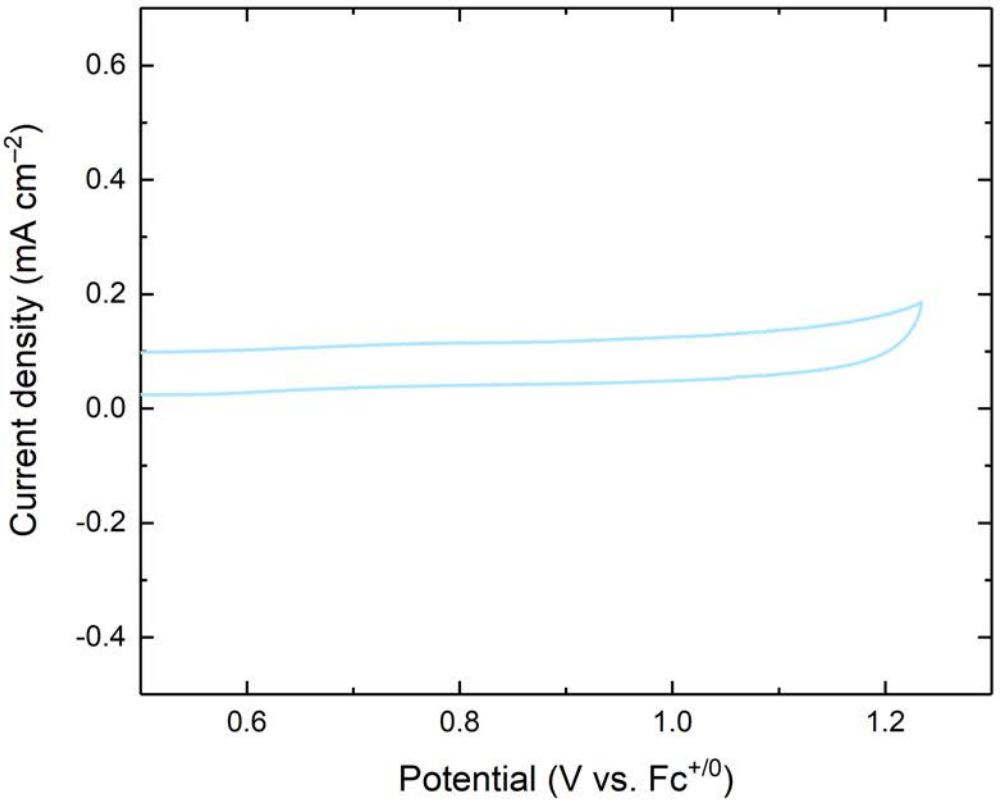

Figure S50. CV of chloride oxidation region of **2** (CH_3CN, 0.1 M [$^nBu_4N$][PF_6], 100 mV/s).

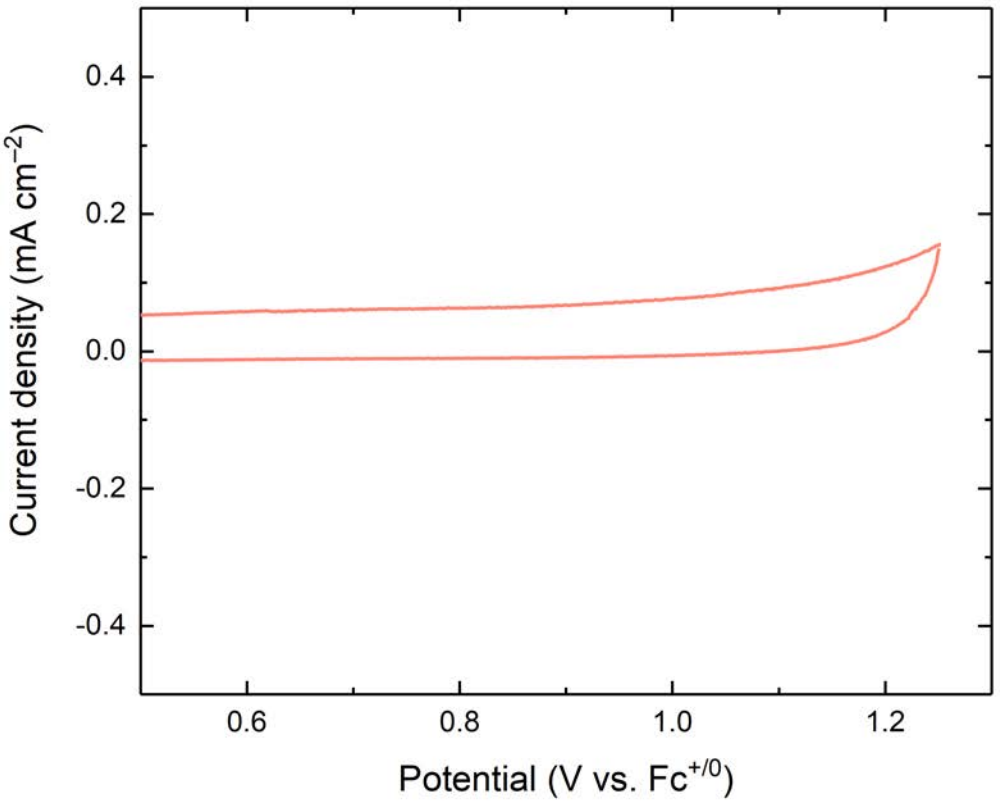

Figure S51. CV of chloride oxidation region of **1-NCCH$_3$** (CH_3CN, 0.1 M [$^nBu_4N$][PF_6], 100 mV/s).

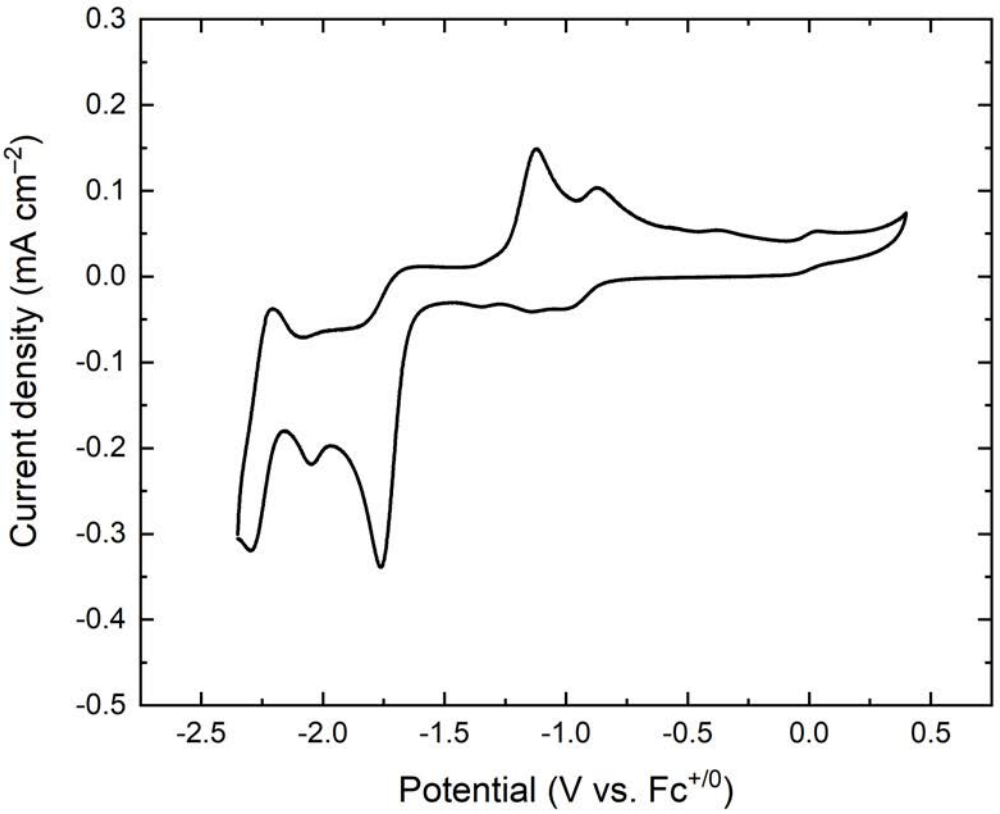

Figure S52. Cyclic voltammetry of **3** (CH_3CN, 0.1 M [$^nBu_4N$][PF_6], 100 mV/s)

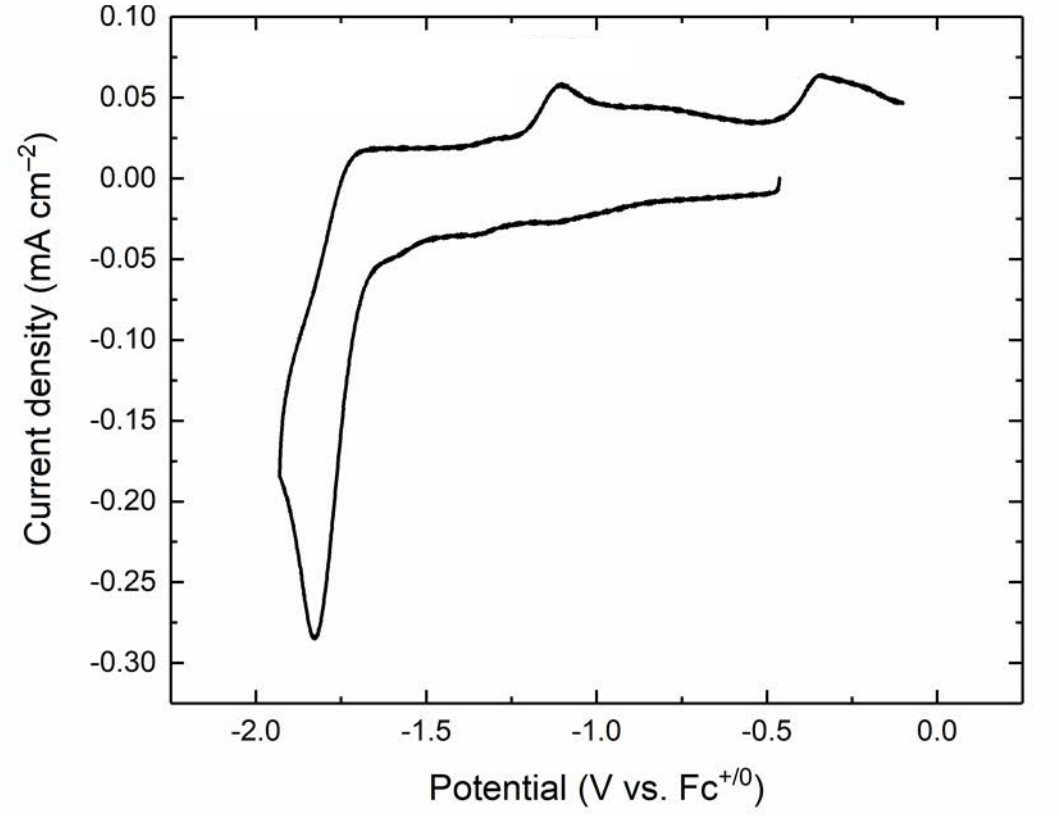

Figure S53. Cyclic voltammetry of **3** (CH_3CN, 0.1 M [$^nBu_4N$][PF_6], 4000 mV/s).

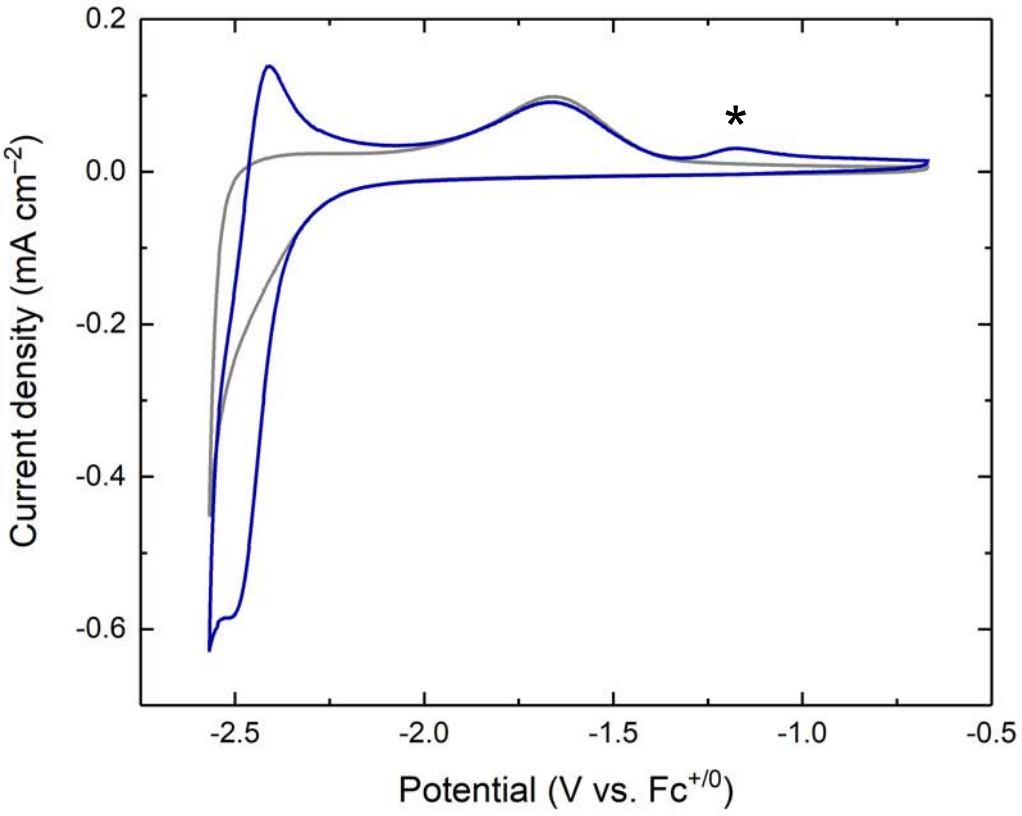

Figure S54. Cyclic voltammetry of PQN (CH_3CN, 0.1 M [$^nBu_4N$][PF_6], 100 mV/s) (*) denotes an anodic, electrode-based process resulting from cathodic scanning to rather negative potentials.

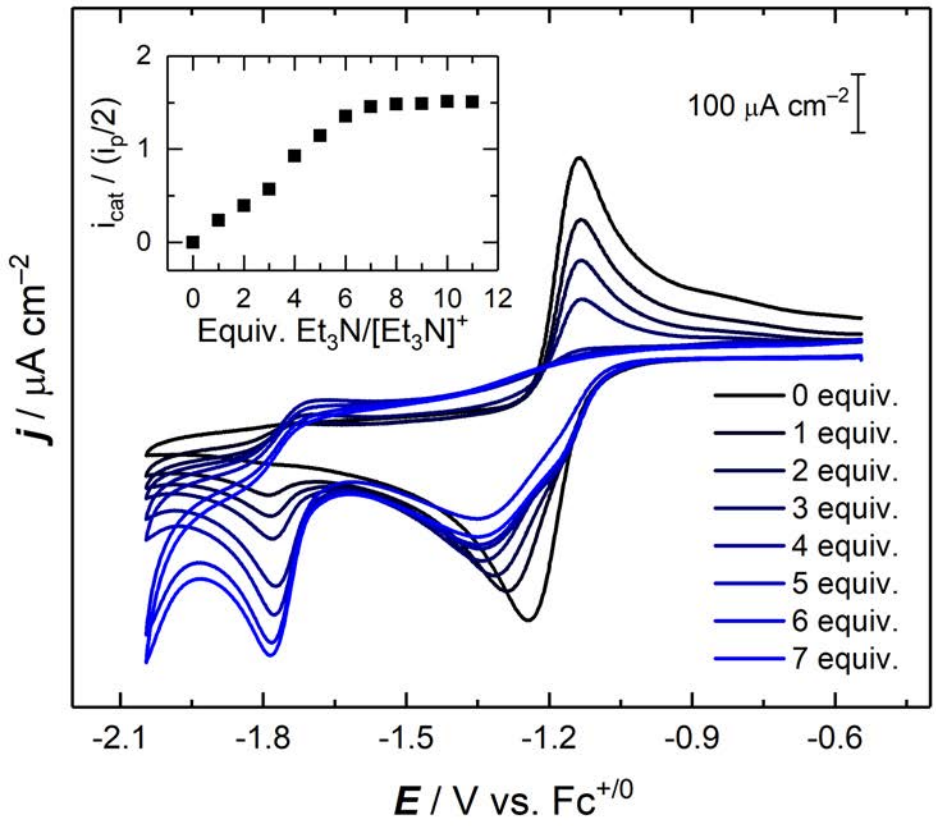

Figure S55. Cyclic voltammetry of **1-Cl** with 1 equv. of $[Et_3NH]^+/Et_3N$ in 50μL additions (CH_3CN, 0.1 M $[^nBu_4N][PF_6]$, 100 mV/s). (Inset): Plot of $i_{cat}/(i_{p/2})$ vs equivalents (mMol) of $[Et_3NH]^+/Et_3N$ added.

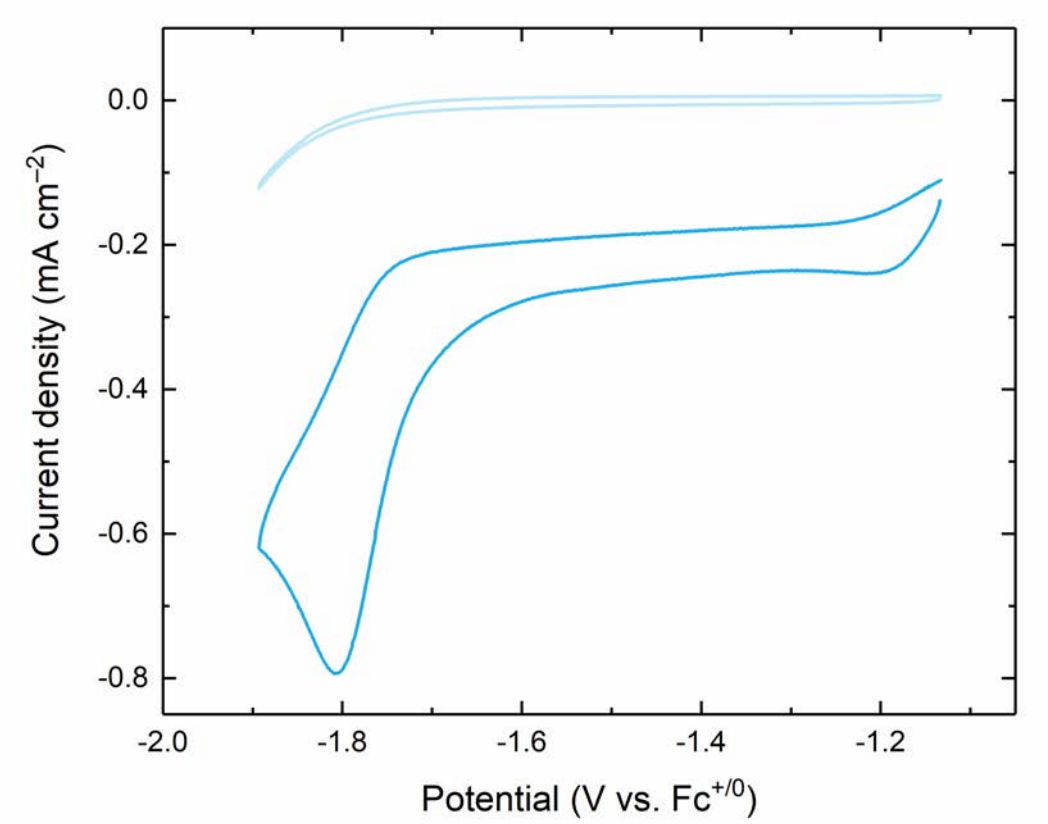

Figure S56. Cyclic voltammetry of $Et_3NH^+OTf^-$ (top); **1-Cl** and 1 equiv. of $Et_3NH^+OTf^-$ (bottom) (CH_3CN, 0.1 M [$^nBu_4N$][PF_6], 100 mV/s).

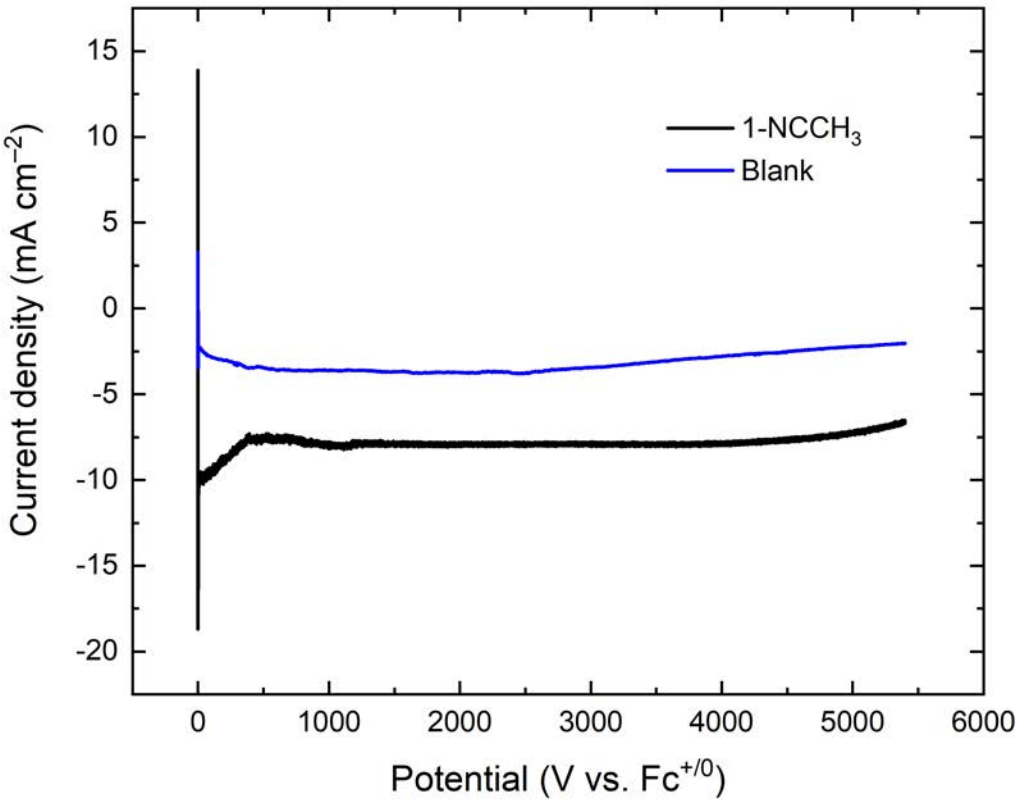

Figure S57. Chronoamperometry experiments conducted during bulk electrolyses with 1 mM **1-NCCH$_3$** plus acid (black line) and an acid-only blank (blue line). Polarization at –1.75 V vs $Fc^{+/0}$. Ten equivalents of ferrocene included as sacrificial reductant, and 10 equivalents of $[Et_3NH]Br$ added as the acid. Supporting electrolyte was 0.1 M $[^nBu_4N][PF_6]$ in each case.

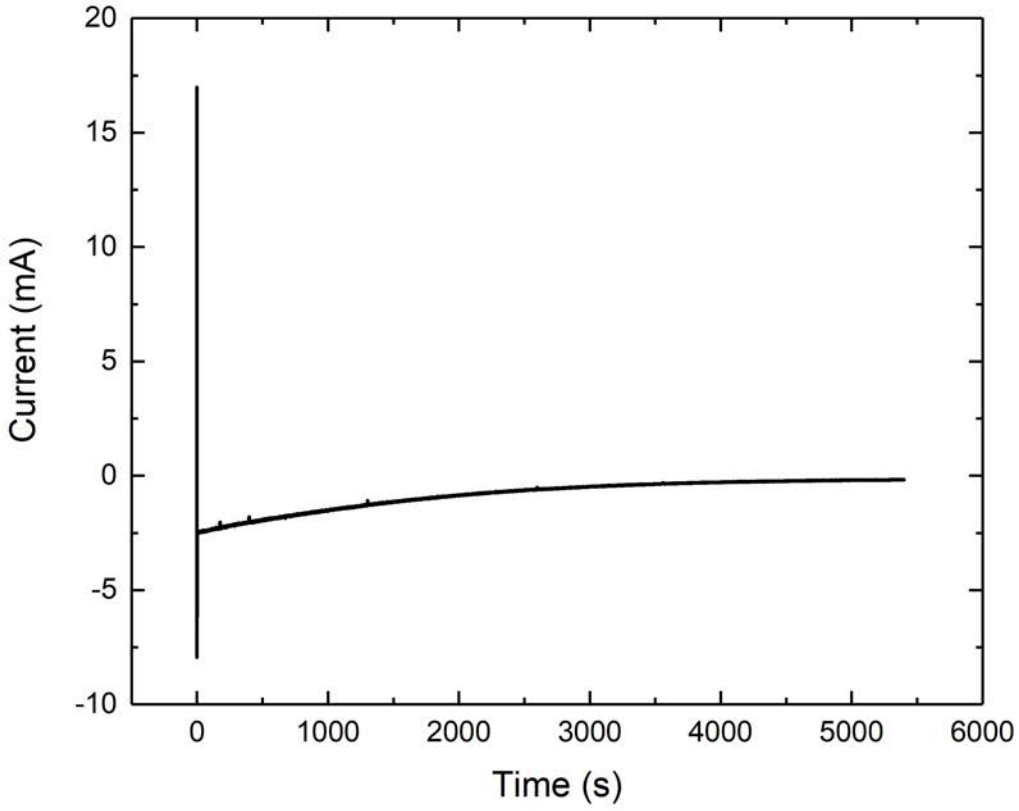

Figure S58. Bulk electrolysis data for **3** polarized at –1.75 V (CH_3CN, 0.1 M [$^nBu_4N$][PF_6]).

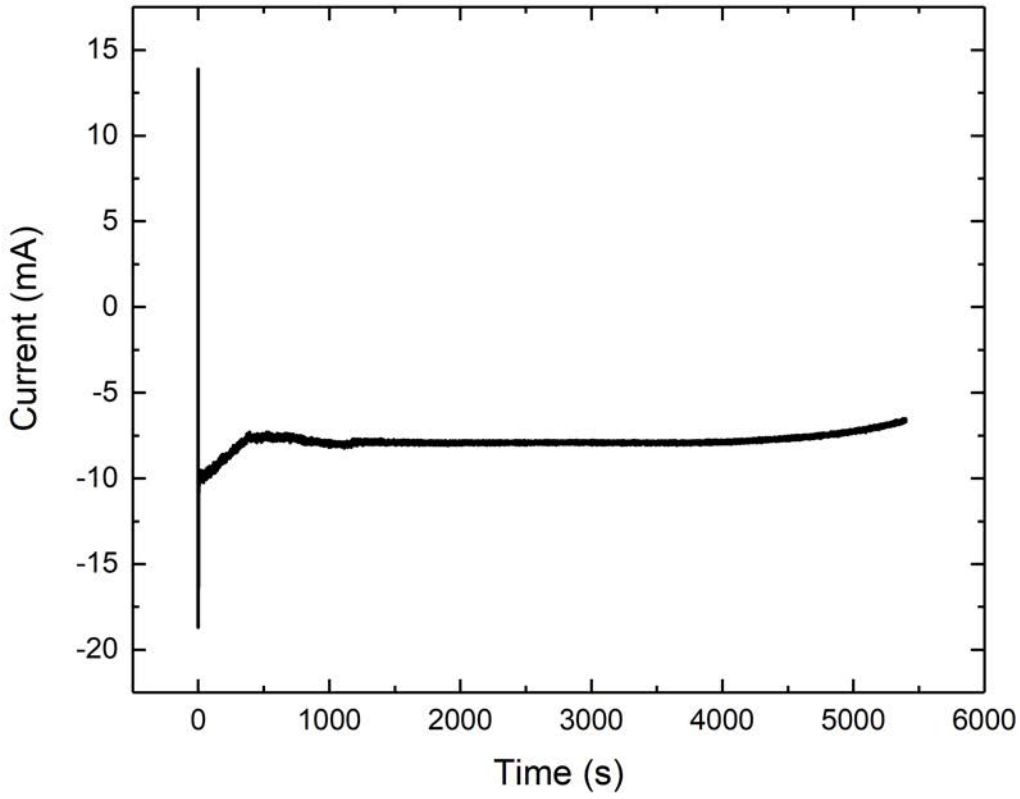

Figure S59. Bulk electrolysis data for **1-NCCH$_3$** with 10 equiv. of $Et_3NH^+OTf^-$ polarized at –1.75 V (CH_3CN, 0.1 M [$^nBu_4N$][PF_6], 100 mV/s).

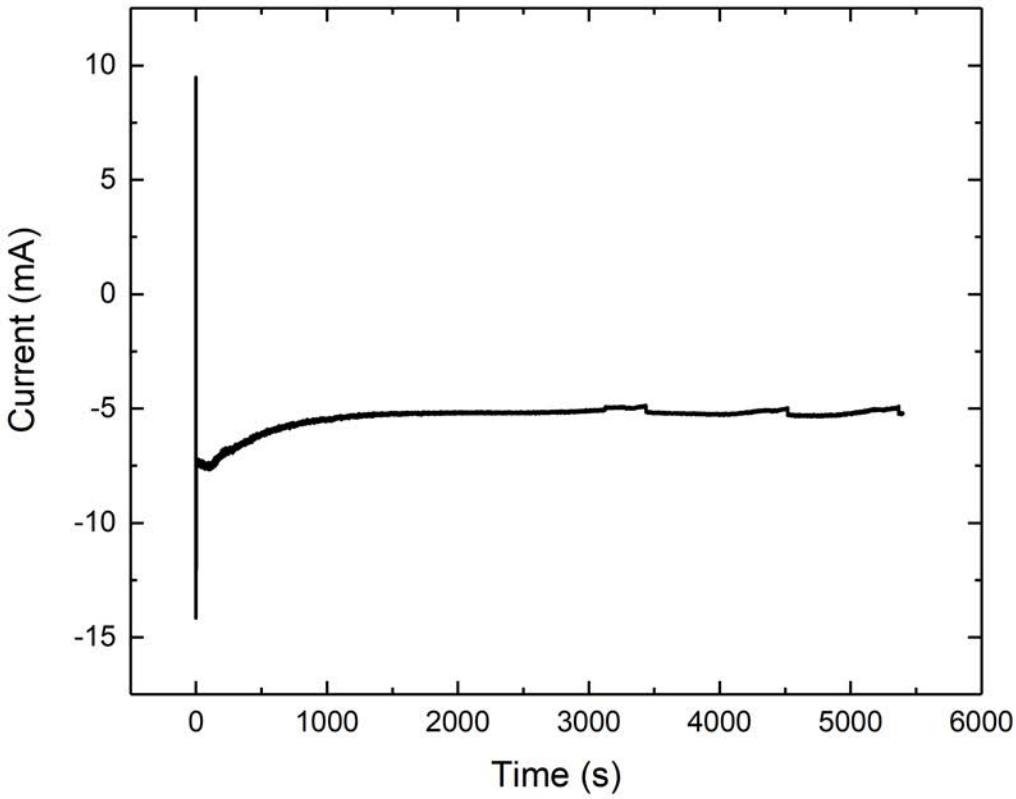

Figure S60. Bulk electrolysis data for **1-Cl** with 10 equiv. of $Et_3NH^+OTf^-$ polarized at –1.75 V (CH_3CN, 0.1 M [$^nBu_4N$][PF_6], 100 mV/s).

X-ray crystallography

*Refinement Details for **1-Cl, 2** and **3**.*

Sets of diffraction data [16617 (**1-Cl**), 25594 (**2**) and 17776 (**3**) reflections using 1º-wide ω- or ϕ-scan frames with scan times of 4-6 seconds (**1-Cl**), 5 seconds (**2**) or 4-6 seconds (**3**)] were collected[1] for single-domain crystals of **1-Cl**, **2**, and **3** using monochromated Cu Kα radiation (λ=1.54178 Å) on a Bruker Proteum Single Crystal Diffraction System with dual CCD detectors and associated Helios high-brilliance multilayer optics and a shared Bruker MicroSTAR microfocus Cu rotating anode x-ray source operating at 45 kV and 60 mA. Data for both compounds were collected with an Apex II CCD detector. The integrated data were corrected empirically for variable absorption effects using equivalent reflections.[2] The Bruker software package SHELXTL was used to solve both structures using "direct methods" techniques.[3] All stages of weighted full-matrix least-squares refinement were conducted using F_o^2 data using the Olex software package[4] equipped with SHELXTL XL v2014.[5] Final crystallographic details are summarized in Table S1.

In the structure of **3**, the Rh-bound hydride ligand (H41) was located as residual electron density in the Fourier difference map; it was therefore included in the model as an isotropic atom and its position was freely refined.

Table S1. Crystal and Refinement Data for $[Cp^*Rh(QPN)(Cl)]^+$ [OTf] (**1-Cl**), [Cp*Rh(QPN)] (**2**) and $[Cp^*Rh(QPN)(H)]^+$ [OTf] (**3**).

	1-Cl	**2**	**3**
CCDC number	1858635	1858633	1858634
Empirical formula	$C_{32}H_{31}ClF_3NO_3PRhS$	$C_{31}H_{31}NPRh$	$C_{32}H_{32}F_3NO_3PRhS$
Formula weight	735.97	551.45	701.52
Temperature	199.99	296.15	199.99
Wavelength	1.54178	1.54178	0.71073
Crystal system	monoclinic	monoclinic	triclinic
Space group	$P2_1/n$	$P2_1/n$	P-1
a	12.9399(2) Å	9.0754(2) Å	10.5485(9) Å
b	15.7672(3) Å	17.3941(4) Å	10.5301(9) Å
c	15.3994(3) Å	16.7425(4) Å	14.8517(12) Å
a	90	90	70.4770(10)
β	94.0144(6)	101.7270(10)	76.8720(10)
γ	90	90	82.9990(10)
Volume	3134.17(10) $Å^3$	2587.78(10) $Å^3$	1512.3(2) $Å^3$
Z	4	4	2
Density (calculated)	1.560 g/cm^3	1.415 g/cm^3	1.541 g/cm^3
Absorption coefficient	6.747 mm^{-1}	6.053 mm^{-1}	0.739 mm^{-1}
F(000)	1496.0	1136.0	716.0
Crystal size	0.14 × 0.085 × 0.045 mm^3	0.17 × 0.085 × 0.03 mm^3	0.24 × 0.23 × 0.08 mm^3
Theta range	8.036 to 140.37	7.41 to 140.456	3.97 to 61.508
Index ranges	$-14 \le h \le 15$, $-18 \le k \le 18$, $-15 \le l \le 18$	$-10 \le h \le 8$, $-20 \le k \le 21$, $-20 \le l \le 18$	$-14 \le h \le 15$, $-14 \le k \le 15$, $-21 \le l \le 21$
Reflections collected	16617	25594	17776
Independent reflections	5720 [R_{int} = 0.0311, R_{sigma} = 0.0311]	4692 [R_{int} = 0.0276, R_{sigma} = 0.0208]	8957 [R_{int} = 0.0380, R_{sigma} = 0.0681]
Absorption correction	Multi-scan	Multi-scan	Multi-scan
Max. and min. transmission	0.7533, 0.5664	0.839, 0.426	0.943, 0.842

Refinement method	Full-matrix least-squares on F^2	Full-matrix least-squares on F^2	Full-matrix least-squares on F^2
Data / restraints / parameters	5720/0/393	4692/0/313	8957/0/452
Goodness-of-fit on F^2	1.072	1.094	0.914
Final R indices [I>2σ(I)]	R_1 = 0.0325, wR_2 = 0.0837	R_1 = 0.0212, wR_2 = 0.0536	R_1 = 0.0466, wR_2 = 0.1251
R indices (all data)	R_1 = 0.0342, wR_2 = 0.0852	R_1 = 0.0217, wR_2 = 0.0539	R_1 = 0.0728, wR_2 = 0.1485
Largest diff. peak and hole	1.24 and -0.76 $e^-/Å^3$	0.30 and -0.41 $e^-/Å^3$	1.35/-0.98 $e^-/Å^3$

[a] $R1\ \Sigma||F_o|-|F_c|| / \Sigma|F_o|$ [b] $wR2 = [\ \Sigma\ [w(F_o^2-F_c^2)^2] / \Sigma\ [w(F_o^2)^2]\ ]^{1/2}$

Table S2. Selected Bond Lengths for **1-Cl, 2 and 3**.

Bond	**1-Cl**	**2**	**3**
Rh–Cl	2.3784(9)	—	—
Rh–P	2.260(9)	2.1744(4)	2.2486(8)
Rh–N	2.140(3)	2.0294(13)	2.093(3)
Rh–Cp*	1.830	1.917	1.862
Rh–H41	—	—	1.48(4)

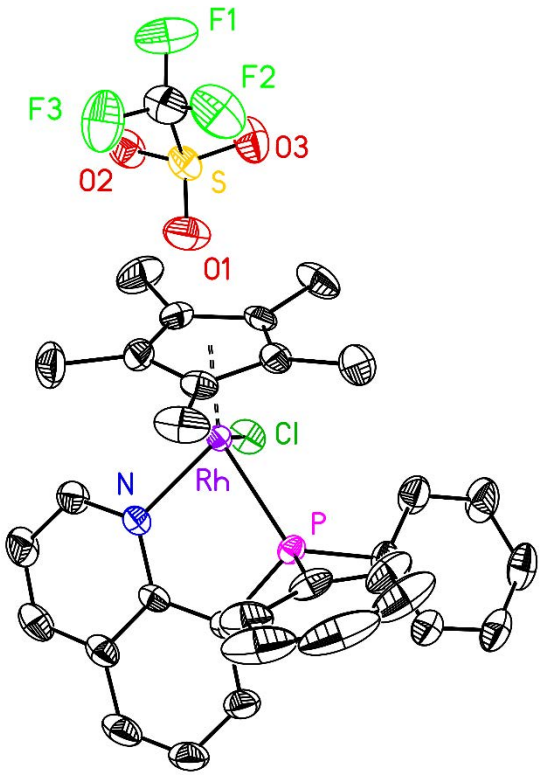

Figure S61. Full solid-state structure of **1-Cl**. Hydrogen atoms omitted for clarity. Displacement ellipsoids shown at the 50% probability level.

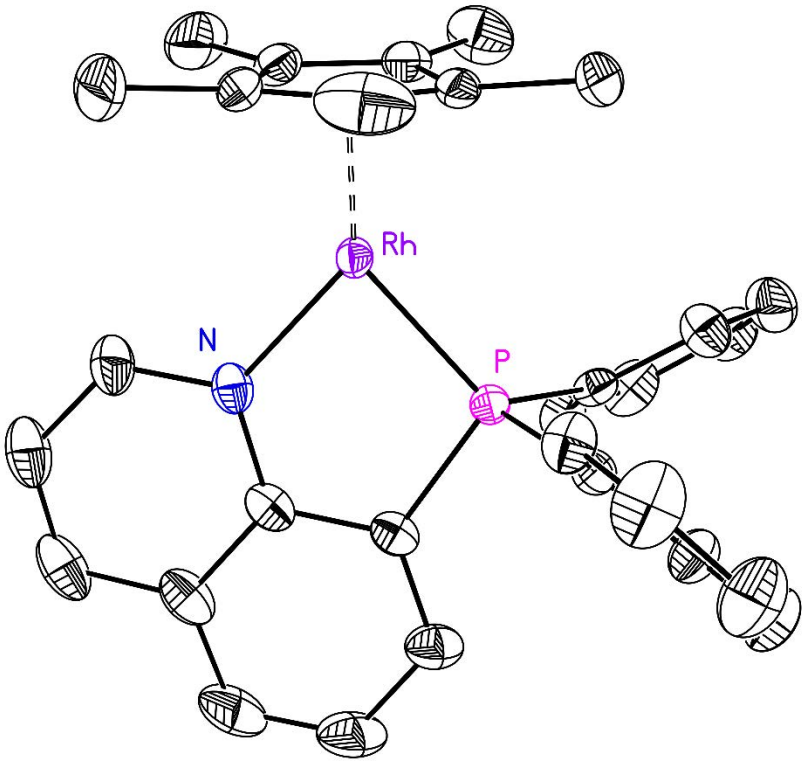

Figure S62. Full solid-state structure of **2**. Hydrogen atoms omitted for clarity. Displacement ellipsoids shown at the 50% probability level.

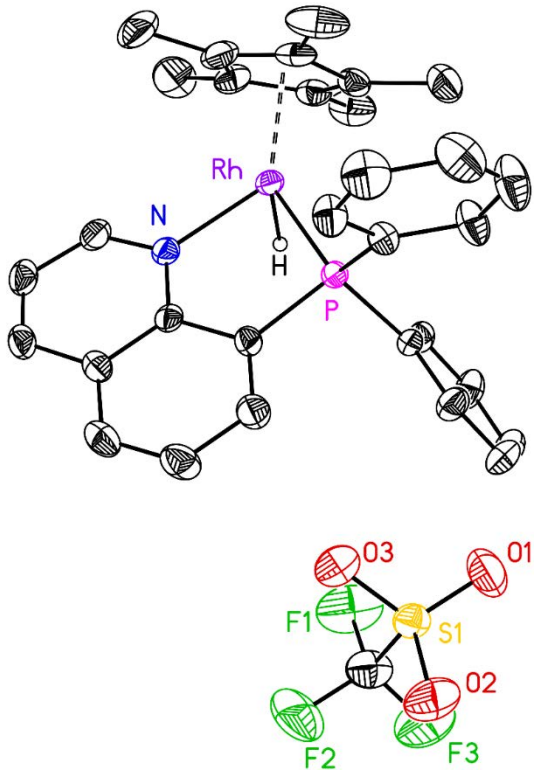

Figure S63. Full solid-state structure of **3**. Hydrogen atoms except for H41 omitted for clarity. Displacement ellipsoids shown at the 50% probability level.

References

1. *APEX2, Version 2 User Manual, M86-E01078,*. Bruker Analytical X-ray Systems: Madison, WI, June 2006.

2. Sheldrick, G. M. *SADABS (version 2008/1): Program for Absorption Correction for Data from Area Detector Frames*, University of Göttingen2008.

3. Sheldrick, G., SHELXT - Integrated space-group and crystal-structure determination. *Acta Crystallogr., Sect. A: Found. Crystallogr.* **2015,** *71*, 3-8.

4. Dolomanov, O. V.; Bourhis, L. J.; Gildea, R. J.; Howard, J. A. K.; Puschmann, H., OLEX2: a complete structure solution, refinement and analysis program. *J. Appl. Crystallogr.* **2009,** *42*, 339-341.

5. Sheldrick, G., Crystal structure refinement with SHELXL. *Acta Crystallogr., Sect. C: Cryst. Struct. Commun.* **2015,** *71*, 3-8.